UiT The Arctic University of Norway

Faculty of Science and Technology

Department of Physics and Technology

On the Linkage Between Rossby Waves and Heatwaves

Jakub Petříček

FYS-3900 Master's Thesis in Physics, Spring 2023

Abstract

This thesis examines the relationship between upper-level atmospheric circulation and heatwaves. We studied the role of planetary Rossby waves in the observed increase in intensity, frequency, and duration of extreme temperature events in the mid-latitudes. Focusing on the summer season, we tested the proposed hypothesis that links recent changes in the Rossby wave amplitudes and propagation speed to the increased occurrence of extreme events. We applied a Fourier decomposition technique to separate the large-scale Rossby waves, defined a fitting amplitude-like metric, and developed a peak-tracking algorithm to estimate their zonal propagation speed.

Heatwaves were identified using a percentile-based definition that enables a straightforward comparison of heatwave magnitude across different regions. We carried out a statistical analysis of the Rossby wave speeds and amplitudes during heatwaves and formulated a hypothesis regarding the latitude-dependent circulation mechanisms that potentially favor heatwaves.

We found that heatwaves in the southern mid-latitudes are more often associated with a low-amplitude setting and non-disrupted zonal flow, while heatwaves in the northern mid-latitudes are accompanied by high-amplitude Rossby waves. We confirmed that this trend further intensified in the last decade. Our analysis did not reveal any overall hemispheric trends in the Rossby wave speed or amplitudes. We did, however, find significant regional trends that possibly affect the heatwave activity through the proposed mechanism.

Acknowledgements

I would like to thank my supervisor Rune Grand Graversen for his valuable ideas and for his navigation through the maze of scientific research. Our meetings and conversations shaped this thesis and made it possible.

I am grateful to my family and my parents for encouraging me in my passion for knowledge, and for their continuous support throughout my studies, both in the Czech Republic and here in Norway. *Děkuju vám.*

A big thanks to my friends in Tromsø, who made the last two years an experience of a lifetime, one full of skiing and adventures. I offer my sincere gratitude to the workers of Tromsø kommune bydrift, who diligently tracked the skiløyper. You too have made this ride smoother. *Takk skal dere ha.*

And finally, thank you, Cooper, for your help with LaTeX, for reminding me to eat regularly, and for being there for me when things got hard.

Contents

Abstract **i**

1 Introduction **1**
1.1 The circulation hypothesis . . . 2
1.1.1 Previous research . . . 3
1.2 Theoretical background . . . 4
1.2.1 Thermal wind . . . 4
1.2.2 Rossby waves . . . 5

2 Data and methods **9**
2.1 ERA5 global reanalysis dataset . . . 9
2.2 Fourier decomposition of the geopotential field . . . 10
2.2.1 Approximation of the geopotential and the wave amplitudes . . . 10
2.2.2 Peak tracking and the wave speed . . . 14
2.3 Heatwave detection . . . 16

3 Results **21**
3.1 Overall changes in amplitude and speed . . . 21
3.1.1 Results of the speed analysis . . . 22
3.1.2 Results of the amplitude analysis . . . 25
3.2 Changes in amplitudes and speed during heatwaves . . . 26
3.2.1 Results of the speed analysis . . . 28
3.2.2 Results of the amplitude analysis . . . 30
3.2.3 Early-period and late-period heatwaves . . . 33

4 Discussion and conclusion **35**
4.1 Results interpretation . . . 35
4.2 Different methodological approaches . . . 36
4.2.1 Identifying Rossby wave characteristics . . . 36
4.2.2 Heat wave selection . . . 37
4.3 Future research . . . 38
4.4 Conclusion . . . 39

A Trends in GP amplitudes **41**

B Propagation speed of high-amplitude waves **45**

C Speed trends in early- and late-period heatwaves **49**

List of figures

1.1 Arctic amplification measured by thickness anomaly, which is highest during the cold months of the year. Figure taken from an article by Francis and Vavrus [14]. 5

1.2 Rossby wave propagation mechanism. The horizontal line represents the original material line aligned around a circle of latitude. An initial disturbance displaces it to the solid line labeled with $t = 0$. The velocity field associated with ζ further advects the fluid parcels in the direction denoted by the arrows, inducing the wavy westward movement. The figure is taken from [26] 7

2.1 A pronounced Rossby wave at 500 hPa stretching far north. Blue and purple colors signalize a higher wind speed. This screenshot was taken on 28 April 2023 from windy.com [30] 10

2.2 A plot of Z_{500} and GP1–5 on a randomly selected day. The blue line is GP1–5, the sum of the first five terms of the Fourier series. We see that GP1–5 correctly captures the overall shape of the geopotential height field, but doesn't include the small height perturbations. 12

2.3 GP1 and GP1–5 daily amplitudes and corresponding monthly climatologies, calculated at 50°N, both at 500hPa and 850hPa levels 13

2.4 GP1–5 on the first three days of July 2022 at 50°N 14

2.5 A relative frequency histogram for the number of peaks that contribute to the GP1–5 speed estimate 15

2.6 GP1–5 speed during summer 2022 at 50°N. Note that 600 km/day corresponds to roughly 7 m/s. 16

2.7 Maximum daily temperatures and the percentile-based climatology used to determine the duration of the 2010 Russian heatwave. The heatwave days are marked by the red line. 18

2.8 HWMId plot for the Russian heatwave that took place between 7 July 2010 and 13 July 2010, with the maximum HWMId value of 86 18

2.9 Duration and HWMId value of the strongest heatwave that occurred every year per latitude and averaged over a latitude range 56°– 60 °N. Other latitude bands show similar results. 19

3.1 QQ plots of GP1–5 speed at 500 hPa for different latitudinal ranges 23
3.2 QQ plots of GP1–5 speed at 850 hPa for different latitudinal ranges 24
3.3 Histograms comparing the distributions of the 1981–2010 data and 2011–2022 data. Corresponding probability density functions were calculated using Gaussian kernel density estimation. 25
3.4 QQ plots of GP1–5 peak-to-peak amplitudes at 500 hPa for different latitudinal ranges 26
3.5 QQ plots of GP1–5 peak-to-peak amplitudes at 850 hPa for different latitudinal ranges 27
3.6 QQ plots of GP1–5 speed at 500 hPa for different latitudinal ranges during heatwaves 28
3.7 QQ plots of GP1–5 speed at 850 hPa for different latitudinal ranges during heatwaves 29
3.8 Mean difference between GP1-5 speed during heatwave periods and non-heatwave periods, expressed in km/day. 30
3.9 QQ plots of GP1–5 peak-to-peak amplitudes at 500 hPa for different latitudinal ranges during heatwaves. 31
3.10 QQ plots of GP1–5 peak-to-peak amplitudes at 850 hPa for different latitudinal ranges during heatwaves. 32
3.11 Mean difference between GP1-5 peak-to-peak amplitudes during the heatwave periods and outside of the heatwave periods, expressed in meters. . . 32
3.12 QQ plots of GP1–5 peak-to-peak amplitudes at 500 hPa for different latitudinal ranges during early-period (1979–2010) and late-period heatwaves (2011-2022). 33
3.13 QQ plots of GP1–5 peak-to-peak amplitudes at 850 hPa for different latitudinal ranges during early-period (1979–2010) and late-period heatwaves (2011-2022). 34

A.1 GP3 amplitudes at 500 hPa show the most pronounced changes from all individual waves. 42
A.2 GP2 amplitude at 500 hPa showing an opposite trend to GP1–5. 43

B.1 Comparison of the speed distributions of high-amplitude and lower-amplitude waves at 500 hPa. Notice the differences are highly visible in both tails, showing that both westward and eastward propagation is affected. 46
B.2 Comparison of the speed distributions of high-amplitude and lower-amplitude waves at 850 hPa. The decreasing tendency is most visible in the eastward propagation speed. 47

C.1 Comparing the distributions of GP1–5 speed at 500 hPa on the heatwave days of the early period (1979–2010) and the late period (2010-2022). . . . 49
C.2 Comparing the distributions of GP1–5 speed at 850 hPa on the heatwave days of the early period (1979–2010) and the late period (2010-2022). . . . 50

Chapter 1

Introduction

Heatwaves are prolonged periods of extremely hot weather, often with little to no rainfall. Frequently dismissed as merely an uncomfortable seasonal phenomenon, heatwaves in fact pose a significant threat to public health, affect the economy, and challenge our way of life. Their devastating impact on society should not be underestimated, especially in a warming world, where the events considered extreme today might become the norm in the upcoming decades.

While we can adapt the existing infrastructure to better resist extreme heat, we cannot adapt our bodies. Exposure to high temperatures can lead to heat exhaustion, dehydration, and life-threatening heatstrokes. Elderly people, young children, and those with pre-existing medical conditions are especially vulnerable. The UN has estimated that the two deadliest heatwaves of the last 20 years, the 2003 European heatwave and the 2010 Russian heatwave, had a combined death toll of over 120 thousand [12], and as recently as in 2022, WHO reported over 15 thousand excess deaths in Europe caused by extremely hot weather [29].

Even though it might seem that Europe is being affected particularly hard, it is likely that the high share of heatwave-related deaths is a result of better reporting systems, and the death toll in other regions is thus undercounted [12]. Moreover, people living in wealthier societies have better access to drinking water, air conditioning, and other resources that provide relief from the harmful effects of heat. It is expected that heatwaves and climate change in general will promote the already existing economic and social inequality.

Drought is closely linked to heatwaves. The UN estimated the worldwide economic costs of drought to be $128 billion over the last 20 years [12]. However, this is likely not the final figure due to the gaps in records reported by underdeveloped countries. The economic losses stem mainly from reduced work productivity and disrupted agricultural production leading to lower crop yields [20]. Furthermore, heatwaves affect the natural water cycle and threaten the drinking water supply. Water shortage can also negatively impact electricity generation from hydropower [21] as well as other energy sources, since power plants often use river water as a cooling medium [8].

In conclusion, heatwaves pose significant risks to society as a whole, making it crucial to study their causes and impacts. As global temperatures continue to rise, it is likely that heatwaves will become more frequent and severe, underscoring the importance of

continued research in this area. By developing a better understanding of the causing mechanisms, we can improve our forecasting abilities, learn more about the character of extreme events in the future, and take steps to prevent and mitigate their impacts.

1.1 The circulation hypothesis

There is agreement that the probability of heatwave occurrence is likely to increase due to anthropogenic climate change [10] [18]. While the exact mechanisms of this process are far from being fully understood, the thermodynamically-driven global warming caused by rising levels of greenhouse gases has been identified as a key reason for the increasing severity of certain types of extreme events, such as heat waves, droughts, and floods [10] [18] [4].

The projected change in global average temperature is expected to directly impact the magnitude of future heatwaves. However, a linear argument simply linking more powerful heatwaves to the temperature increase might not sufficiently explain the full picture, as it could lead to an underestimate of other, non-linear effects, whose relationship to the global temperature increase is not as straightforward.

Changes in atmospheric dynamics are hypothesized to contribute to the occurrence of temperature extremes as part of this non-linear effect. With the dynamic drivers of extreme heat acting on top of the well-established response to the rising greenhouse gas levels, the risk of life-threatening heatwaves is exacerbated. The combined effects lead to extremes that cannot be explained solely by the positive radiative forcing induced by the increased concentration of greenhouse gases.

The hot tail of the temperature distribution has shifted more toward the extremes in comparison to the mean, suggesting that there are unforeseen complex processes affecting weather variability other than the observed temperature increase [11]. In this thesis, we use reanalysis data to investigate one of the suspected mechanisms, changes in atmospheric circulation. We further attempt to establish a relationship between these changes and the occurrence of summer heat waves in the mid-latitudes.

It has been well observed that the current global warming is not happening at the same rate across all latitudes [7]. The Arctic regions undergo faster warming compared to the mean global rate. This effect is known as Arctic amplification and it possibly has significant implications for the characteristics of the zonal atmospheric flow [11]. A hypothesis that received attention both from the scientific community [1] and the media [28], is the circulation hypothesis. Proposed in 2012 by Francis and Vavrus [14], the hypothesis connects Arctic amplification to changes in the properties of atmospheric waves and, further, links these changes to extreme weather events. As Arctic amplification reduces the meridional temperature gradient, this in turn decreases the speed of zonal winds through the thermal wind relation. The zonal flow is responsible for advection of weather systems, and with the circulation becoming more stationary, the surface weather conditions become longer-lasting and their impact is therefore enhanced.

The mid-latitude atmospheric circulation patterns are characterized by synoptic-scale cyclones and large-scale planetary waves known as Rossby waves. The Rossby waves contribute to the overall heat transfer in the atmosphere by carrying heat from the tropics

toward the poles and, conversely, cold air toward the equator [17] [15], thus influencing the local weather conditions. Elongation of the Rossby wave amplitudes in the meridional direction is another hypothesized change that would widen the range of latitudes that can be affected. This thesis investigates the changes in the wave amplitudes during heatwaves to see if a significant correlation between high amplitude days and extreme surface temperatures can be established.

According to Rossby wave theory [26], Rossby wave phase speed is related to the velocity of the zonal winds. Some of the recent observational analyses suggest that the velocity of the zonal jet stream is decreasing [13] [9], and several modeling studies have succeeded in finding a causal link between Arctic warming and a weaker mid-latitude jet stream [1]. The combined arguments hint at a possible decrease in the Rossby wave eastward propagation speed due to Arctic amplification. The purpose of this thesis is thus to explore the questions inherent to the circulation hypothesis within the framework of summer heatwaves through statistical data analysis. We examine the changes in the atmospheric circulation patterns and the trends of both wave amplitudes and phase speeds.

1.1.1 Previous research

We provide a quick overview of the previously published research. In their first article on the circulation hypothesis [14], Francis and Vavrus focused on the deceleration of the eastward progression of the Rossby waves and the increase in their amplitude. The study was regionally constrained to North America and North Atlantic. The authors directly linked the previously observed zonal wind reduction to slower wave propagation. By selecting a narrow range of 500 hPa contour lines and tracking them over the whole study region, they captured the wave pattern in the geopotential height field. Their analysis confirmed a northward elongation of the wave amplitudes. Their results showed considerable seasonal differences both in the amplitude and speed trends that the authors explained by the seasonal differences in Arctic amplification, which reaches its maximum during the cold months of the year, as shown in Fig. 1.1. Therefore many following studies focused on the influence of Arctic amplification on mid-latitude winter weather [5] [7].

The results of Francis and Vavrus were disputed on the basis of sensitivity to the methodology used. In her 2013 article, Barnes argued that the dynamic changes presented in the previous study were not supported by observations [2]. Francis and Vavrus revisited the circulation hypothesis again in 2015, assessing trends in the frequency of occurrence of high-amplitude days in several selected regions and in the whole Northern Hemisphere [13]. They concluded that the high-amplitude days are becoming more frequent in most of the studied regions, however, due to substantial regional and seasonal variability, determining a significant mean hemispheric effect is challenging.

Despite the ambiguity of the early results, the circulation hypothesis became widely popular among the scientific community as well as the general public [28]. Individual extreme events were directly attributed to the hypothesized effects of Arctic warming [5] [31]. However, several following studies failed to find a robust correlation between Arctic amplification and atmospheric blocking responsible for persistent weather conditions [3], overall hemispheric trends in the Rossby wave phase speed [22] or their amplitudes [4].

Significant regional wave trends were confirmed in relation to extreme weather events characterized by persistent temperature and precipitation anomalies [25]. To investigate

the role of Arctic warming, observed regional changes in the zonal propagation of weather systems during summer months have been recently positively correlated to the decreasing meridional temperature gradient. The following modeling attempts to determine a causal relationship between Arctic warming and the future character of these changes have however been inconclusive [19]. Now our thesis will follow, investigating the summer heatwaves and taking inspiration from the prior studies.

This brief overview of the previous research shows that the results are often divergent or even contradictory. Moreover, proving causality using observations alone is difficult since distinguishing a forced response from the natural atmospheric variability presents a major obstacle. With only about 40 years of sufficiently accurate observational records, we cannot simply rule out the possibility that the observed changes are no more than manifestations of the internal year-to-year or decadal variability.

Nonetheless, there is strong model evidence that Arctic warming can indeed impact the atmospheric flow and surface weather in the mid-latitudes [1], justifying the research in this area. An assessment of past changes, the main objective of this thesis, is just as important as finding out more about the mechanisms that will be affecting the climate system in the future.

1.2 Theoretical background

1.2.1 Thermal wind

The Arctic regions are on average warming more than twice as fast as the lower latitudes, owing to a variety of factors, some of them also being linked to changes in atmospheric circulation and energy transport [15]. Nevertheless, most sources mention sea ice loss and the decrease in spring and summer snow cover as the main driving mechanisms, inducing positive feedback by exposing the land areas and oceans, and thus lowering the surface albedo [6].

Arctic amplification can be measured by comparing the change in surface temperature in the Arctic relative to the mean hemispheric change. However, for the purposes of quantification of the effects of Arctic amplification on atmospheric circulation, a different metric can be used, based on the temporal differences in the 1000 – 500 hPa thickness. The thickness Z of a layer, defined by the hypsometric equation [17]

$$Z = Z_{p_2} - Z_{p_1} = \frac{R}{g_0}\overline{T}\ln\left(\frac{p_1}{p_2}\right), \tag{1.1}$$

is the difference in geopotential height of two isobaric surfaces, and it is proportional to the mean layer temperature $\overline{T}$. The thickness has increased more in the Arctic than in other regions, proving that the meridional temperature gradient has decreased throughout the whole layer. This is a more relevant metric due to its association with the thermal wind relation [13]

$$\vec{v_T} = \vec{v_g}(p_2) - \vec{v_g}(p_1) = \frac{R}{f}\ln\left(\frac{p_1}{p_2}\right)\hat{z} \times \nabla\overline{T}. \tag{1.2}$$

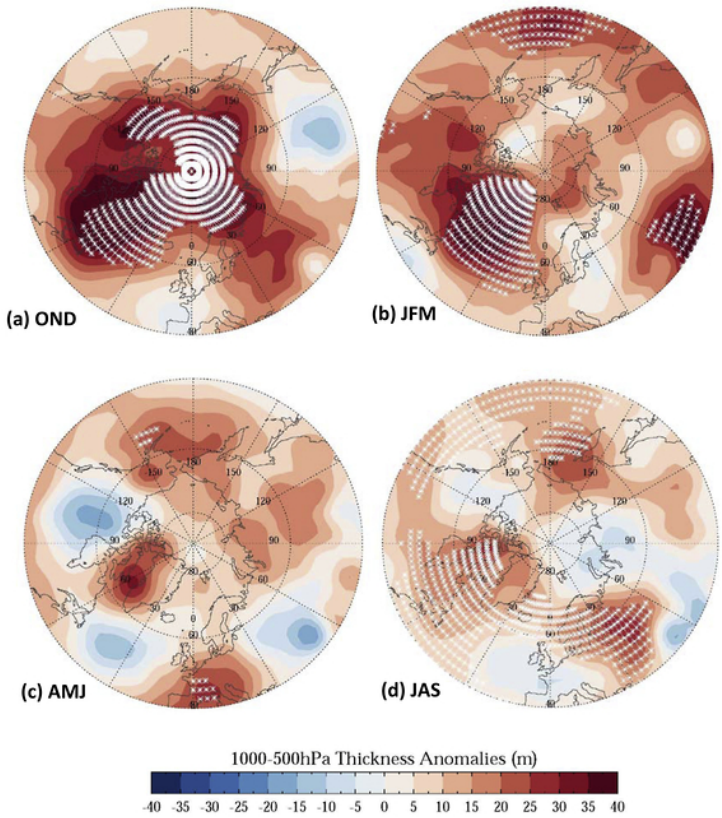

Figure 1.1: Arctic amplification measured by thickness anomaly, which is highest during the cold months of the year. Figure taken from an article by Francis and Vavrus [14].

Based on hydrostatic and geostrophic balance, the thermal wind $\vec{v}_T$ is obtained as a vector difference in the geostrophic wind at two pressure levels p_1 and p_2, and since the jet stream at 500 hPa is generally considered to be almost geostrophic, a decrease in the magnitude of $\vec{v}_T$ directly translates to a decrease in the jet stream velocity. The equation (1.2) shows the importance of the decrease in the temperature gradient $\nabla\overline{T}$, which exists due to the natural difference in solar insulation between the high and low latitudes, and which is affected by Arctic amplification, although with strong seasonal differences that can be seen in Fig. 1.1.

1.2.2 Rossby waves

We identify the driving forces that give rise to the Rossby waves and we examine some of their important dynamical properties. To overcome the inherent complexity of fluid dynamics and to gain insight into the processes occurring in the mid-latitude atmospheric flow, we make several simplifying assumptions: we will work within the shallow water quasi-geostrophic framework. Even with these strong assumptions, the results turn out to be relevant to the real atmospheric processes.

One of the assumptions of the quasi-geostrophic theory is that at the lowest order, the flow is geostrophic and therefore horizontally non-divergent. This allows us to define a stream function $\psi(x, y)$ that describes the horizontal velocity field at the lowest order as

$$u = -\frac{\partial\psi}{\partial y}, \quad v = \frac{\partial\psi}{\partial x}$$

Vorticity plays the most important role in the formation of Rossby waves. It is the measure of spin in a fluid. We define relative vorticity $\vec{\omega}$ as the curl of the velocity vector,

$$\vec{\omega} = \nabla \times \vec{v}.$$

For a large-scale atmospheric flow, only the vertical component of $\vec{\omega}$ is of interest [17]. Therefore it is given a new symbol,

$$\zeta = \partial_x v - \partial_y u = \nabla^2 \psi$$

Conventionally, ζ is also called relative vorticity. Absolute vorticity η is defined as

$$\eta = \zeta + f,$$

where ζ is the relative vorticity f is the Coriolis parameter, also known as the planetary vorticity.

Earth's rotation induces a natural planetary vorticity gradient, which in the mid-latitudes can be approximated using the β-plane approximation

$$f(y) = f_0 + \beta y.$$

In every theory, it is useful to identify conserved quantities, as they provide insight into the fundamental principles that govern a system, and often allow us to derive prognostic equations that describe it. The prognostic equation related to the large-scale Rossby waves is the potential vorticity equation, which under the shallow water quasi-geostrophic assumptions simplifies to

$$\frac{D}{Dt}\left(\zeta + f - \frac{\psi}{L_D^2}\right) = 0, \tag{1.3}$$

where $\frac{D}{Dt} = \partial_t + \vec{v} \cdot \nabla$ is the material derivative operator and L_D is the Rossby radius of deformation. The term in parentheses is the potential vorticity, and the equation simply states that it stays constant during the fluid's motion.

For the sake of simplicity, we will further assume that L_D is very large (larger than the horizontal length scale L). Then the last term in (1.3) can be neglected, resulting in

$$\frac{D}{Dt}\Big(\zeta + f\Big) = 0, \tag{1.4}$$

The equation (1.4) presents the never-ending tug of war between the relative and planetary vorticity. There is a naturally present planetary vorticity gradient that exists due to Earth's rotation, and therefore any change in the value of f of a fluid parcel due to its displacement must result in a change of ζ, so that the absolute vorticity η is conserved.

The basic Rossby wave propagation mechanism can be described as follows: imagine a material line consisting of fluid parcels carried by a background zonal flow, aligned along a circle of latitude with $\zeta = 0$ at a time t_0. Now suppose a fluid parcel is displaced in the meridional direction. This changes the value of f, but according to (1.4), the potential vorticity, which in our case is equal to the absolute vorticity, must be conserved. Thus, the displacement of a fluid parcel results in a change in the relative vorticity ζ, a positive one for a southward displacement and a negative one for a northward displacement.

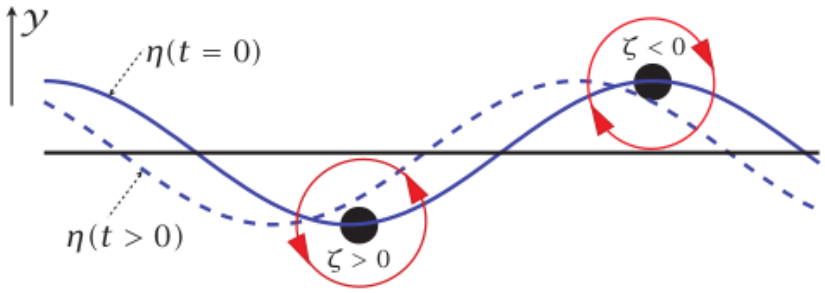

Figure 1.2: Rossby wave propagation mechanism. The horizontal line represents the original material line aligned around a circle of latitude. An initial disturbance displaces it to the solid line labeled with $t = 0$. The velocity field associated with ζ further advects the fluid parcels in the direction denoted by the arrows, inducing the wavy westward movement. The figure is taken from [26] .

The induced velocity field makes the fluid parcels oscillate back and forth around their original latitude, and the now wavy material line propagates to the west in the form of a Rossby wave (see Fig. 1.2). In the Earth's atmosphere, the displacement originates from longitude-dependent differences in diabatic heating or it can be induced by topography, such as the Rocky Mountains or the Himalayas. The resulting waves are the long Rossby waves with low wave numbers, and they will be the subject of our study.

We can derive the dispersion relation for Rossby waves by looking for a wave-like solution to (1.4). The solution can be found by linearizing around a mean flow. For a flow on a mid-latitude β-plane, the potential vorticity equation (1.4) turns into

$$\left(\frac{\partial}{\partial t} + u\frac{\partial}{\partial x} + v\frac{\partial}{\partial y}\right)\zeta + \beta v = 0. \tag{1.5}$$

Assume that the flow consists of a constant background zonal flow plus a perturbation in the horizontal direction:

$$u = \bar{u} + u', \quad v = v', \quad \zeta = \partial_x v' - \partial_y u' = \zeta',$$

The perturbation terms u' and v' and their derivatives are assumed to be small compared to the background flow. We can now set in the prescribed forms of u, v, and ζ into (1.5) and linearize the result by neglecting the products of perturbation quantities, keeping only the linear primed terms, since the magnitude of the non-linear terms is negligible. The final form of (1.5) in terms of the stream function ψ' is then

$$\left(\frac{\partial}{\partial t} + \bar{u}\frac{\partial}{\partial x}\right)\nabla^2\psi' + \beta\frac{\partial\psi'}{\partial x} = 0. \tag{1.6}$$

This equation can be solved analytically by seeking a wave-like solution

$$\psi' = \mathrm{Re}[\tilde{\psi}\exp(i\phi)],$$

where $\phi = kx + ly - \omega t$ and k, l are the zonal and meridional wave numbers, respectively. Setting in the assumed solution and solving for $\omega = \omega(k, l)$ yields

$$\omega = \bar{u}k - \frac{\beta k}{k^2 + l^2}.$$

The zonal phase speed c_x^p is given by

$$c_x^p = \frac{\omega}{k} = \bar{u} - \frac{\beta}{k^2 + l^2}. \tag{1.7}$$

and the zonal group speed c_x^g is calculated by differentiating ω with respect to k,

$$c_x^g = \frac{\partial \omega}{\partial k} = \bar{u} - \frac{\beta\left(l^2 - k^2\right)}{\left(k^2 + l^2\right)^2}. \tag{1.8}$$

The zonal phase speed is always westward relative to the mean background flow $\bar{u}$, in line with the mechanism shown by Fig. 1.2. Because $\bar{u}$ tends to be westerly and greater than $\beta/(k^2 + l^2)$, the zonal phase speed c_x^p is usually westerly too. However, for long Rossby waves with low wave numbers k and l, the phase speed c_x^p can occasionally become zero or negative, meaning that the Rossby waves are stationary relative to the Earth's surface, or are even moving westward. This possibly has serious implications for the duration of surface weather conditions. In our analysis, we will use reanalysis data to determine c_x^p of Rossby waves, and we will seek a possible strengthening of extreme events due to a negative trend in c_x^p.

Chapter 2
Data and methods

2.1 ERA5 global reanalysis dataset

In this thesis, we used the ERA5 reanalysis dataset produced by the European Centre for Medium-Range Weather Forecast (ECMWF) [16]. It is a comprehensive, high-resolution dataset containing gridded data of a large number of atmospheric, ocean-wave, and land-surface variables from 1979 onward. The dataset is created using a process called data assimilation that is based on combining weather observations and state-of-the-art weather prediction models.

During the data assimilation process, a computer model is run using the best available estimate of the current atmospheric state as the initial condition, and a weather forecast for a given time period is generated. In the next step, observational data from the same time period, such as satellite measurements, surface observations, and weather balloon data, are combined and used to correct the weather forecast. The objective is to obtain a consistent and continuous description of the atmosphere that closely resembles reality. This updated state is called the analysis, and it is used as the initial condition for the computer model in the next time step of the data assimilation process. ERA5 is a reanalysis dataset, which is a comprehensive collection of analyses that reach back decades and are all results of the same data assimilation algorithms.

For the purpose of studying heat waves, the ERA5 2m temperature was used. Additionally, the 500 hPa and 850 hPa geopotential height datasets were utilized to analyze Rossby wave patterns. The datasets consist of daily data with a spatial resolution of 0.5° latitude by 0.5° longitude. Although the patterns are more pronounced at the 500 hPa level where the large-scale flow is not significantly influenced by Earth's surface and synoptic-scale weather systems, all findings were tested at the 850 hPa level to examine their continuity across different altitudes.

2.2 Fourier decomposition of the geopotential field

2.2.1 Approximation of the geopotential and the wave amplitudes

To identify Rossby waves, their amplitudes, and movement, we analyzed the 500 hPa and 850 hPa geopotential height fields. The Rossby wave pattern can be seen as large alternating areas of high and low geopotential height (Fig. 2.1). When the field contours show large-scale deviations from their non-disturbed orientation, which is parallel to the lines of latitude, it is likely due to a Rossby wave influencing the large-scale atmospheric circulation, bringing temperature and pressure anomalies into the region.

Our approach to analyzing the Rossby wave amplitudes and their movement was fundamentally different from the one of Francis and Vavrus and other studies [14] [2]. Francis and Vavrus studied the amplitude of Rossby waves by tracking a narrow range of contours of constant geopotential height. Instead of considering the contour lines stretching over a large region, we identified the local waviness tendency of the geopotential height field at each latitude separately. Further, we assumed a simple relationship between the vertical wavy pattern observed in the individual latitudinal anomalies of the geopotential height, and the spatial extent of the Rossby wave in the meridional direction, spanning a much wider range of latitudes. By assessing the long-term trends in the waviness of the geopotential height latitude by latitude, we sought to investigate the hypothesized changes in the overall meridional extent of Rossby waves.

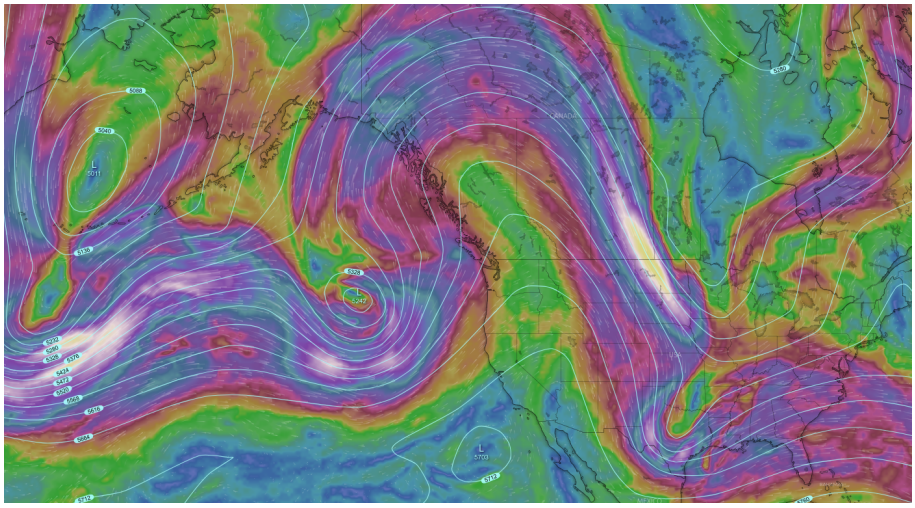

Figure 2.1: A pronounced Rossby wave at 500 hPa stretching far north. Blue and purple colors signalize a higher wind speed. This screenshot was taken on 28 April 2023 from windy.com [30]

We employed a Fourier decomposition technique to split the complex geopotential height field into individual harmonic waves based on the zonal wave number. The Fourier coefficients of the series are used to calculate the amplitudes of the vertical oscillations in the geopotential. The amplitude analysis was carried out for waves with zonal wave number n ranging from 1 to 5. This way, we separated the major constituents of the geopotential field from smaller, synoptic-scale perturbations, whose impact on the Rossby wave shape is mostly local. Throughout this thesis, we will refer to these five simple harmonic functions as GP1 to GP5.

Next, we truncated the Fourier series after five terms and used the sum of the first five waves as an approximation of the geopotential field. We refer to this sum as GP1–5. To analyze trends and changes in the waviness of the geopotential field, we defined an amplitude-like metric of GP1–5 (we make this distinction since it is a different quantity from the amplitude defined using Fourier coefficients) as the difference in meters between the highest peak and the lowest trough of GP1–5. In signal processing, this is often called the peak-to-peak amplitude, and we use this term too.

The geopotential height of an isobaric surface can be described by a smooth function that is periodic with respect to longitude, the period being one revolution around the Earth, i.e. $L = 360°$ of longitude. Such a function can be represented in terms of its Fourier series, which expresses a periodic function as an infinite sum of sines and cosines with unique frequencies and phases.

In the ERA5 dataset, the geopotential height $Z_{500}(t, \phi, \theta)$ of the 500 hPa isobaric surface is given as a function of time, longitude θ, and latitude ϕ. By fixing $t = t_0$ and $\phi = \phi_0$, we are left with $Z_{500}(\theta)$, a periodic function of longitude only. The function $Z_{500}(\theta)$ can be decomposed into its basic frequency components.

The general formula for a Fourier series is

$$Z_{500}(\theta) = \frac{a_0}{2} + \sum_{n=1}^{\infty} \left(a_n \cos\left(\frac{2\pi}{L} n\theta\right) + b_n \sin\left(\frac{2\pi}{L} n\theta\right) \right), \tag{2.1}$$

where $L = 360$ is the period of Z_{500} and the Fourier coefficients a_n and b_n are given by

$$a_n = \frac{2}{L} \int_0^L Z_{500}(\theta) \cos\left(\frac{2\pi}{L} n\theta\right) d\theta, \quad n \in \mathbb{N}_0$$
$$b_n = \frac{2}{L} \int_0^L Z_{500}(\theta) \sin\left(\frac{2\pi}{L} n\theta\right) d\theta, \quad n \in \mathbb{N}.$$

The equation (2.1) represents the sine–cosine formulation of the Fourier series, and it can be equivalently rewritten in an amplitude-phase form

$$Z_{500}(\theta) = \frac{a_0}{2} + \sum_{n=1}^{\infty} \left(A_n \cos\left(\frac{2\pi}{L} n\theta - \varphi_n\right) \right), \tag{2.2}$$

where

$$A_n = \sqrt{a_n^2 + b_n^2}, \quad n \in \mathbb{N},$$
$$\varphi_n = \arctan\left(\frac{b_n}{a_n}\right), \quad n \in \mathbb{N}.$$

are the wave amplitude and the phase shift of the nth harmonic, respectively.

We calculated the amplitudes A_n for n ranging from 1 to 5 for every day of the observation period, 1979 – 2022 summer months (June, July, August – JJA), and for every latitude in the 40°N–60°N range. These amplitudes are referred to as GP1 to GP5 amplitudes. We summed the first five terms of the sum in (2.2), obtaining a representative approximation of the geopotential field. We called this approximation GP1–5. We then calculated the peak-to-peak amplitude of GP1–5 as the difference between the highest peak and the

lowest trough of GP1–5. Figure 2.2 shows an example of how well GP1–5 approximates the actual geopotential field on a randomly selected day. We concluded that GP1–5 captures the overall shape of Z_{500} to a good approximation, excluding the smaller perturbations that we disregarded as redundant for our purposes, and therefore we further used GP1–5 in the analysis of the geopotential height field.

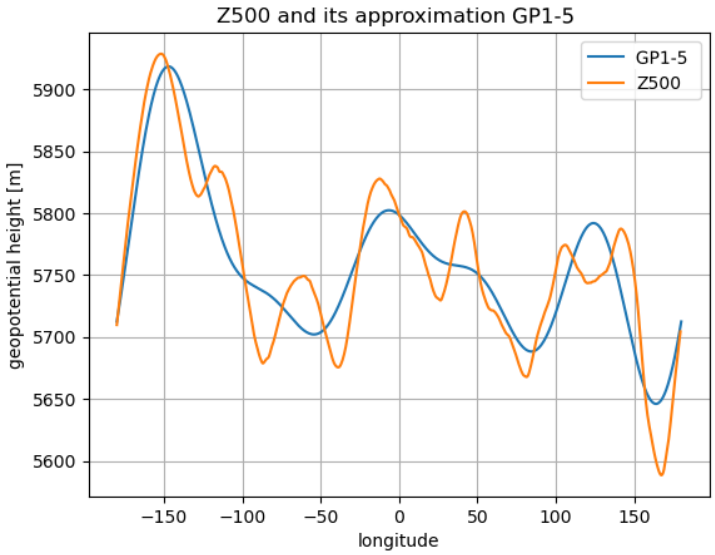

Figure 2.2: A plot of Z_{500} and GP1–5 on a randomly selected day. The blue line is GP1–5, the sum of the first five terms of the Fourier series. We see that GP1–5 correctly captures the overall shape of the geopotential height field, but doesn't include the small height perturbations.

Notice that using our approach, the wave amplitudes A_n, as well as the peak-to-peak amplitude, are functions of time and latitude only, without any longitude dependency, which disappeared by integrating zonally in the calculation of the Fourier coefficients. Therefore our analysis of potential trends in amplitude changes is not constrained to a specific region defined by a longitude range as in other studies [14] [13]. The trends in waviness of the geopotential field were investigated locally, latitude by latitude.

The set of eight panels in Fig. 2.3 shows the frequency distribution of the range of values that the wave amplitudes take on, as well as their corresponding interpolated monthly climatologies. The first two rows (panels a, b and c, d) show GP1 and GP1–5 amplitudes and climatologies at the 500 hPa level, whereas the last two rows (panels c, d and e, f) show the same, but at the 850 hPa level. The climatologies show that there is a clear seasonal cycle of the wave amplitudes of the geopotential field, which are the largest during the winter months when the polar regions receive virtually no sunlight, and the meridional temperature gradient has the greatest magnitude. That leads to greater variability in geopotential height compared to summer.

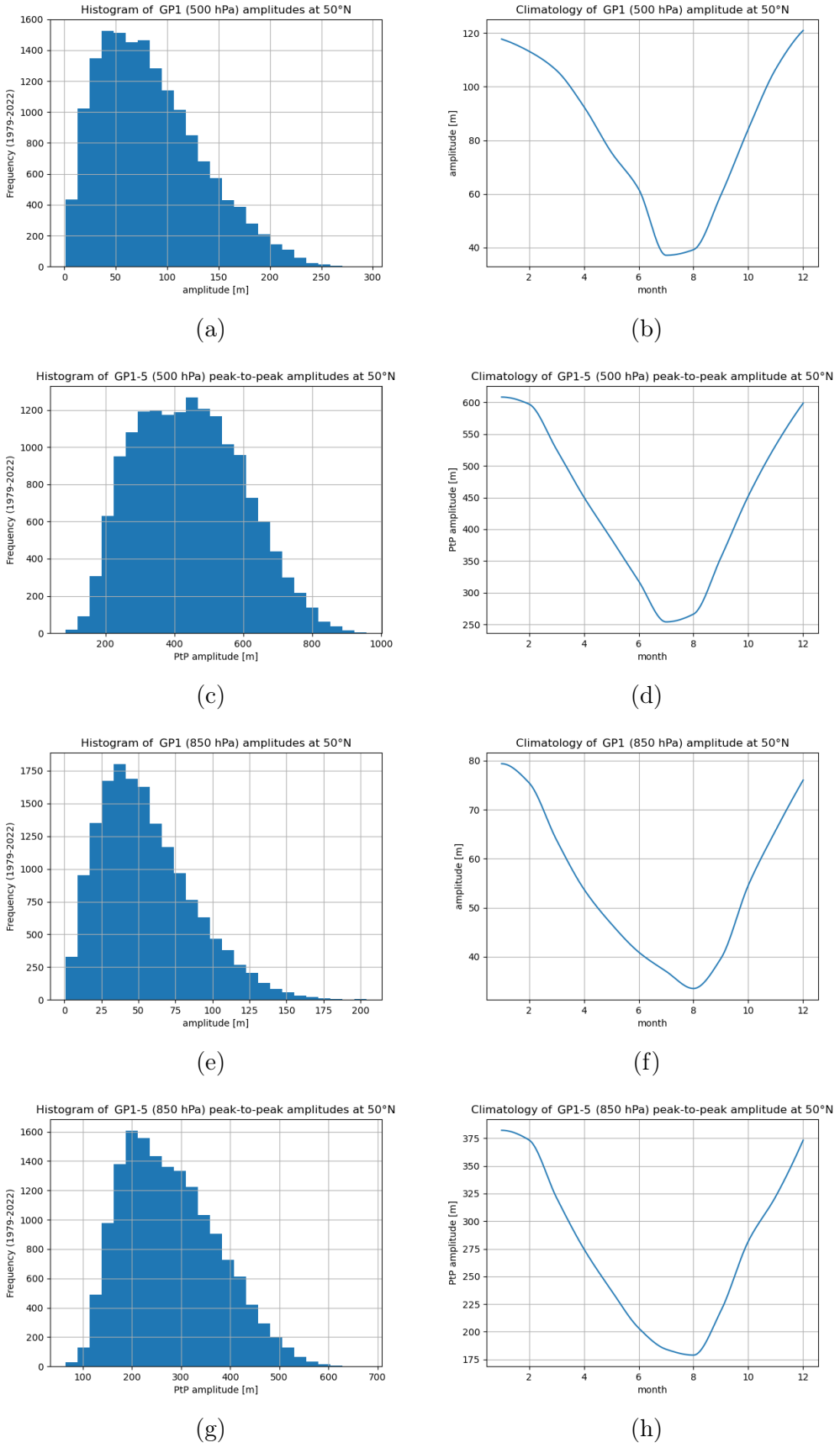

Figure 2.3: GP1 and GP1–5 daily amplitudes and corresponding monthly climatologies, calculated at 50°N, both at 500hPa and 850hPa levels

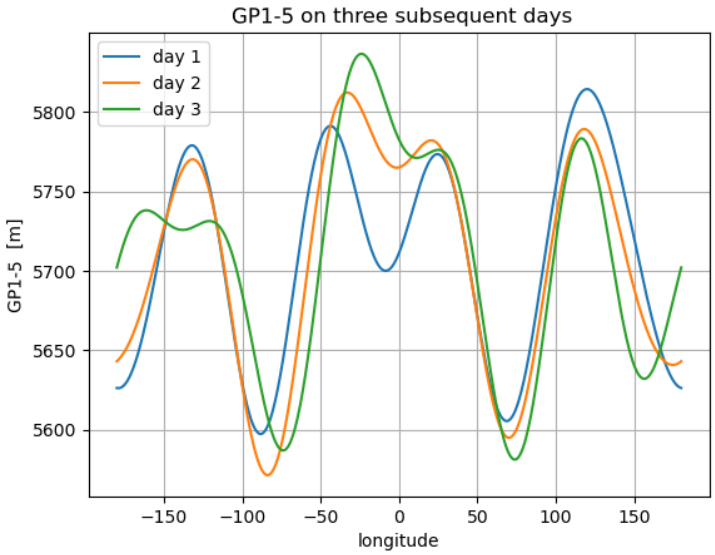

Figure 2.4: GP1–5 on the first three days of July 2022 at 50°N

2.2.2 Peak tracking and the wave speed

We estimated the speed of GP1–5 zonal propagation using a simple peak tracking algorithm. Observing the day-to-day changes in the location of GP1–5 wave peaks, we noticed that their shift is usually continuous on a short time scale, such as one day. Figure 2.4 shows GP1–5 on three subsequent days, the three first days of July 2022, displaying the continuous movement of the peaks.

Our algorithm is based on averaging the peak movement over a 7-day observation window. For each day of the observation period, 1979 – 2022 summer months (JJA), and at each latitude in the 40°– 60°N range, we further continued as follows:

First, we identified all peaks of GP1–5 on the first day of the 7-day window and saved their longitude. Then we proceeded to identify GP1–5 peaks on the following day, and we related them back to the peaks on the previous day. We did this by comparing the longitudes of the peaks. If, on the second day, a peak was found within a region 25° west or east from a peak that was localized on the first day, these two peaks were regarded as the same moving peak, and its day-to-day longitude difference was saved. We repeated this process with the peaks on the third day, matching them to the peaks found on the second day and saving their change in longitude, and so on.

This way, we tracked the original peaks found on the first day throughout the whole 7-day window, saving their day-to-day longitude shifts. The shifts can be interpreted as velocities of the peaks expressed in units of degrees per day. For each of the peaks identified on the first day of the tracking window, we averaged the 7 daily values to obtain a mean speed of the peak over the tracking window. Finally, we once again averaged all the mean speed values of the peaks to get a single number representing the velocity of the overall GP1–5 wave shape during the 7-day period, referred to as the GP1–5 speed. It can be easily converted from degrees per day to km per day by multiplying the GP1–5 speed by $\left(2\pi r_0 \cos(\lambda)\right)/360$, where $r_0 = 6371$ is the mean Earth radius in km and λ is the latitude where the peaks of GP1–5 were tracked. We assigned the GP1–5 speed value to day 4 of the 7-day tracking period.

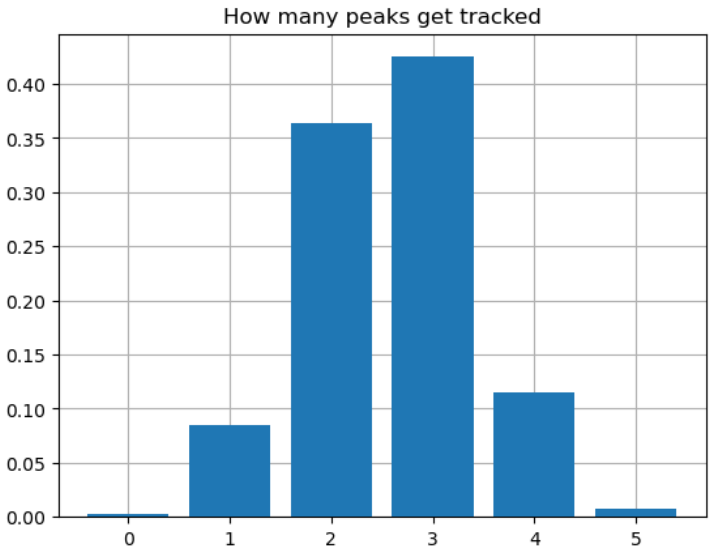

Figure 2.5: A relative frequency histogram for the number of peaks that contribute to the GP1–5 speed estimate

There are naturally several questions that need to be answered, namely whether all peaks of GP1–5 can be tracked in this manner, and, since the number of peaks of GP1–5 can differ from day to day, how many average peak velocities go into the calculation of the final GP1–5 speed. The last question considers the number of days on which the tracking algorithm failed to follow at least a single peak, resulting in a missing value of GP1–5 speed.

Using this algorithm, not every peak can be tracked. We defined several exceptions when that is the case. First, if no nearby peak is found on the following day within the 25° range, that peak cannot be tracked. Similarly, if two peaks are found within the 25° range, the tracking stops. Such a setting can be seen in Fig. 2.4: the leftmost peak breaks into two on day 3, and that will stop the tracking of this peak. Only the peaks that were successfully tracked for the whole 7-day period contribute to the final speed estimate.

The second and third questions are answered by Fig. 2.5. The relative frequency histogram shows that most often, three peaks are tracked and their speed averaged, resulting in the final GP1–5 speed estimate. We also see that the number of days on which no peak was tracked is negligible compared to the whole size of the dataset.

The GP1–5 speed was calculated for every latitude in the 40°– 60° range on every day of the observation period on both 500 hPa and 850 hPa pressure levels. The speed is positive on average, resulting in an eastward motion of GP1–5, in accordance with the direction in which weather systems are usually advected. Fig. 2.6 shows a 3-month-long excerpt from the dataset.

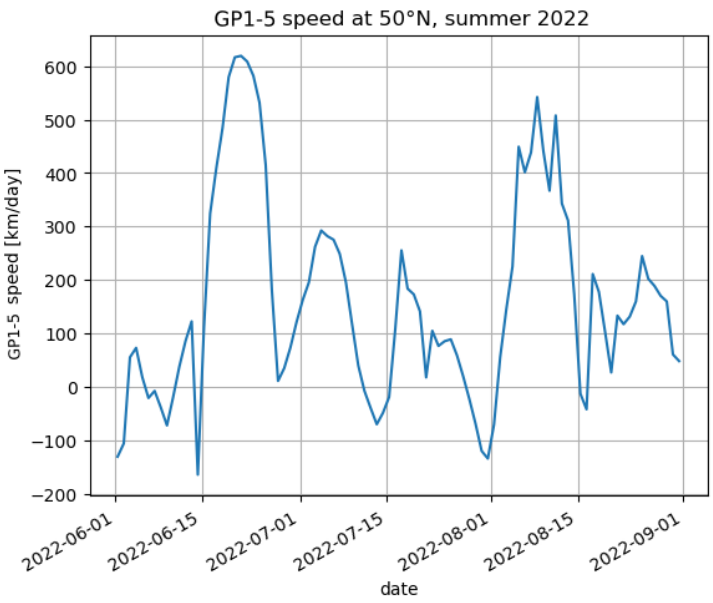

Figure 2.6: GP1–5 speed during summer 2022 at 50°N. Note that 600 km/day corresponds to roughly 7 m/s.

2.3 Heatwave detection

To perform a statistical analysis, large amounts of data are needed. Therefore we employed an algorithmic way of detecting heatwaves within the temperature dataset, proposed by Russo et al. [23], and we were able to obtain enough samples.

In recent decades, vast areas of the world have suffered under extreme heat conditions. However, comparing the severity and magnitude of heat waves across different latitudes is a challenging subject, as the baseline temperature for each such event can vary greatly between regions. Additionally, the impact of a heat wave depends on its duration. Both of these aspects are taken into account by a percentile-based *heat wave magnitude index daily* (HWMId). The index enables a direct comparison of heat waves with different durations and different maximal temperatures across different regions. In their study of the strongest European heatwaves since 1950, Russo et al. [23] demonstrated the potential of their index by providing reports from historical newspapers, showing that HWMId correctly identifies events that are perceived as extreme by the general public.

The idea behind HWMId is to define a heatwave as a period of three and more consecutive days on which the maximum temperature in a given region exceeds a predefined daily threshold. Each day of the heatwave is assigned a daily heatwave magnitude. The daily values are then summed over the whole duration of the identified heatwave, resulting in the final value of HWMId for the heatwave in the given region. This way, both the temperature extremes and the duration are taken into account.

For the purpose of this thesis, we assumed an additional condition not mentioned in the original article: a heat wave is not interrupted if on less than three consecutive days the maximum temperature remains under the daily threshold. It is reasonable to think that the positive impact of a brief cooling period on people's well-being is largely diminished by the continuation of another heat wave. The development in atmospheric circulation

also often lags behind the changes in surface temperature, making our addition to the definition justified for the purposes of a statistical analysis of Rossby wave properties, which do not change as rapidly as the surface temperature.

The process of calculating HWMId consists of two steps: heatwave detection and assignment of heatwave magnitude. First, a percentile-based climatology used for determining heatwave events is established. For a given day of the year d, we selected a temperature dataset A_d defined as

$$A_d = \bigcup_{y=1981}^{2010} \bigcup_{i=d-15}^{d+15} T_{y,i}, \tag{2.3}$$

where $T_{y,i}$ denotes the daily maximum temperature of the day i in the year y. The day d is the center of a 31-day-long time window and A_d is the set of daily maximum temperatures observed within the time window in every year between 1981 and 2010. The year range was selected to be the same as Russo et al. used in their study [23], and we can later verify our calculations by comparing them to their results. The climatology for the day d is set to be the 90th percentile of A_d. By applying this procedure on all days of the year d, we calculated the base climatology for every latitude and longitude grid point. However, we used a land-sea mask to mask out temperatures above the ocean. Whether a day is a part of a heatwave is determined by comparing the maximum daily temperature T_d with the corresponding climatological threshold value, the 90th percentile of A_d. Recall that only three consecutive days above the threshold constitute a heatwave.

Next, to estimate the strength of the heat wave, each heatwave day was assigned a daily heatwave magnitude M_d. T_{30y25p} and T_{30y75p} were calculated as the 25th and 75th percentiles of the dataset

$$\tilde{A} = \bigcup_{y=1981}^{2010} T_y,$$

where T_y is the maximum temperature in the year y. Hence $\tilde{A}$ is a time series consisting of 30 annual maximum temperatures within the reference period 1981–2010. Note that $\tilde{A}$ is independent of the day d. The daily heatwave magnitude M_d is defined as a function of daily maximum temperature T_d

$$M_d(T_d) = \begin{cases} \dfrac{T_d - T_{30y25p}}{T_{30y75p} - T_{30y25p}} & \text{if } T_d > T_{3025p} \\ 0 & \text{if } T_d \leq T_{30y25p} \end{cases} \tag{2.4}$$

The final value of HWMId for a given heatwave is calculated as the sum of M_d for every day d of the heatwave. Defined this way, using region-dependent percentiles, the index enables a direct comparison of heatwaves across latitudes.

Notice that even though the reference climatology based on the 90th percentile of A_d can be used to identify heatwaves during any part of the year, only the summer heatwaves will be assigned an HWMId value due to the condition in the calculation of M_d, since it is unlikely that a warm period during any other season would exceed T_{30y25p}, the 25th percentile of $\tilde{A}$, which contains annual maximum temperatures that occur during summer.

Next, we employed the HWMId calculation in locating the heatwaves and determining their durations. We went through all grid points and found the strongest heatwave from each year based on the HWMId value, leaving us with a maximum of 44 (1979–2022)

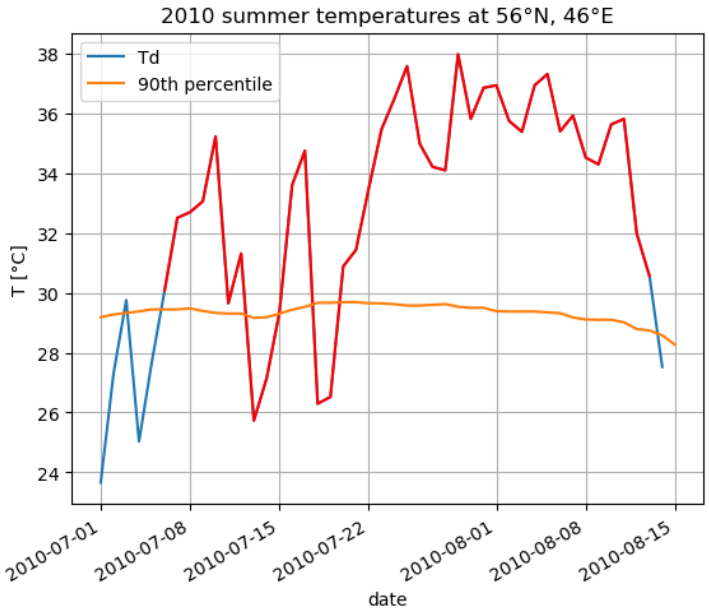

Figure 2.7: Maximum daily temperatures and the percentile-based climatology used to determine the duration of the 2010 Russian heatwave. The heatwave days are marked by the red line.

heatwaves per grid point. We conclude that this is enough heatwave days to conduct a statistical analysis, as the number of samples is sufficient to estimate an underlying probability distribution.

To check our calculations against the results from the original article by Russo et al. [23], we recreated an analysis of a 2010 Russian heatwave. The center of the heatwave was localized at 56°N, 46°E, which is the grid point with the highest HWMId value, 86.4, close to what Russo et al. found in their study. The heatwave in this region started on 7 July 2010 and ended on 13 July 2010. Fig. 2.7 shows the maximum daily temperatures and the base temperature used to determine the duration of the heatwave. The enormous spatial extent of the heatwave, shown in Fig. 2.8, was the same as the one determined by Russo et al., proving that we have successfully recreated the results from the original article [23].

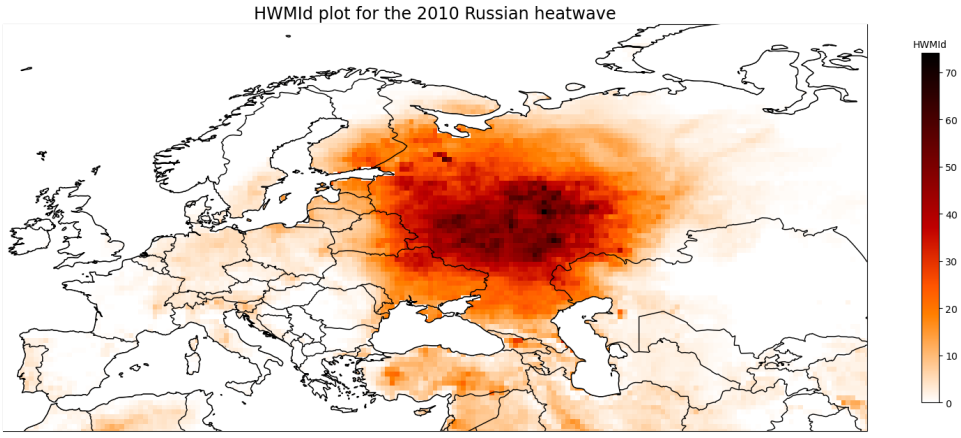

Figure 2.8: HWMId plot for the Russian heatwave that took place between 7 July 2010 and 13 July 2010, with the maximum HWMId value of 86

We show an unrelated, but nevertheless interesting result that can be obtained from our heatwave dataset: by selecting the single strongest heatwave that occurred each year within a selected circle of latitude, we can show that there is an increasing trend both in the duration and the strength of the heatwaves. This result is in line with the findings of other authors, stating that heatwaves have become stronger and more persistent [10] [18]. Fig. 2.9 shows this trend in a range of latitudes from 56°N to 60°N, but the same trend can be observed in the other latitude bands that we studied, which ranged from 40°N to 60°N. Notice the spike in 2010, corresponding to the unprecedented Russian heatwave presented in Figs. 2.7 and 2.8.

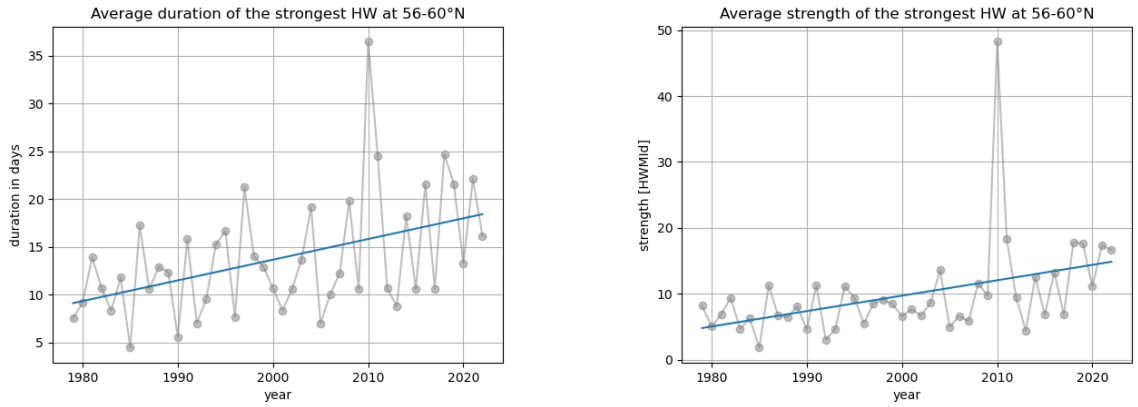

Figure 2.9: Duration and HWMId value of the strongest heatwave that occurred every year per latitude and averaged over a latitude range 56°– 60 °N. Other latitude bands show similar results.

Chapter 3

Results

3.1 Overall changes in amplitude and speed

Our focus was to investigate the possible changes in Rossby wave characteristics over time, particularly during the summer months, evaluate any discernible patterns or trends that may have emerged, and relate them to extreme heatwaves. First, we identified the overall changes without selecting a subset of the data including heatwaves specifically. We inferred the trends in Rossby wave amplitudes from an analysis of GP1 to GP5, the first five harmonic constituents of the decomposed geopotential field, and GP1–5, a sum thereof. An estimate of the wave speed was obtained by a peak tracking algorithm. Both methods were described in the previous chapter. To assess the trends, we compared the Rossby wave amplitudes and speeds during the summer months (June, July, August – JJA) between 2011 and 2022 with those from the previous 30-year-long time period of 1981-2010, which served as the baseline for the comparison. Nevertheless, even with three decades of data from the early period and more than a decade of data from more recent times, a statistical analysis cannot rule out the possibility of the existence of internal atmospheric variations that manifest on a decadal time scale and are in fact not caused by human activity [1].

We chose to present our results using QQ (quantile-quantile) plots. It is a type of probability plot used to compare the underlying probability distributions of two datasets [27]. It is constructed by plotting the quantiles of the datasets against each other. Each point (q_1, q_2) is plotted by calculating the same quantile of both datasets, in our case the early-period speeds and amplitudes, and the recent-period ones. Our QQ plots show the 1st to the 99th percentile in unit steps. To make the plots easier to read, we indicate the top five deciles with a diamond-shaped marker.

By our choice, the x-component of (q_1, q_2) corresponds to a given percentile of the recent-period data, whereas the y-component represents the same percentile, but of the early-period data. Since the plot is constructed only by comparing percentiles, it is a good graphical tool for determining the similarity of two datasets with a different number of samples, provided we have enough samples to estimate the distributions of the data.

If the plotted points follow the straight line $y = x$, it means that $q_1 = q_2$ for all plotted quantiles, and the two datasets contain data with similar values. However, if the plotted

points deviate from the straight line, we say that one of the distributions is skewed compared to the other, either to the left or to the right, depending on which side of the line $y = x$ the points fall. Then, the quantiles of one of the datasets are generally larger than those of the other. This can be the case for the whole dataset, or just selected quantiles. In our plots, often only the top percentiles divert from the straight line, implying that the most extreme values differ across the datasets.

Based on the distance from the line, it can be deduced which quantiles differ the most between the two datasets. In our QQ plots, points lying above the line, that is in the $y > x$ half-plane, signalize a negative change in amplitude in the last decade, whereas points below the line signalize an increase. The same rule applies to the eastward propagation speed. With the westward propagation speed, due to its negative sign, points above the line signalize an increase in westward propagation, and conversely, points below the line signalize a decrease in westward speed in the last decade. The distance from the $x = y$ line was further used as a metric for determining the statistical significance of the results.

We determined the statistical significance of the results using a Monte Carlo simulation. We randomly drew two subsets of the whole dataset, each containing the same number of samples as when constructing the QQ plot. For these subsets, we calculated the corresponding sets of percentiles and the absolute difference between them. This value is referred to as simulated distance since it corresponds to the distance from the line $y = x$ in the QQ plots, which determined the relative skewness of the two distributions. We repeated this process 1000 times to obtain a distribution of simulated distances under the null hypothesis that the distributions of the two datasets are identical. To determine the significance level of the results, we compared the original distance to the simulated distances. If the original distance was larger than 95% of the simulated distances, we concluded that the difference between the datasets was statistically significant at the 95% confidence level. Significant results were plotted in red.

To increase the number of samples, we selected a larger subset of the amplitude (speed) dataset ranging over a wider latitude band. The subset was then averaged to produce an amplitude (speed) time series with one value per day. We tested averaging over a three-degree-wide band, and a five-degree-wide one, both yielding consistent results across the 40°N – 60 °N region. Therefore we only present the plots where the selected subset ranged over five degrees of latitude to reduce the number of plots shown.

The trends in speed distribution were tested at two different pressure levels, 850 hPa and 500 hPa. While the strongest winds associated with Rossby waves are typically found at 500 hPa, and the wave pattern in the geopotential field is more pronounced there, we sought to confirm our findings at 850 hPa too. The geopotential field at this level is comparatively more influenced by synoptic-scale weather systems; however, we eliminated the local perturbations by employing Fourier decomposition in the calculation of GP1–5, which enables us to study the day-to-day changes in the geopotential field with higher precision.

3.1.1 Results of the speed analysis

Figures 3.1 and 3.2 reveal the recent changes in the GP1–5 summer speed distribution by comparing the percentiles of the data from the first thirty years of daily observations (1981–2010, JJA), to the data from the last decade (2011–2022, JJA). In the description

of our results, an increase or decrease always refers to changes that occurred in the last decade. Figure 3.1 shows the changes at the 500 hPa level, while Fig. 3.2 shows the changes at the 850 hPa level.

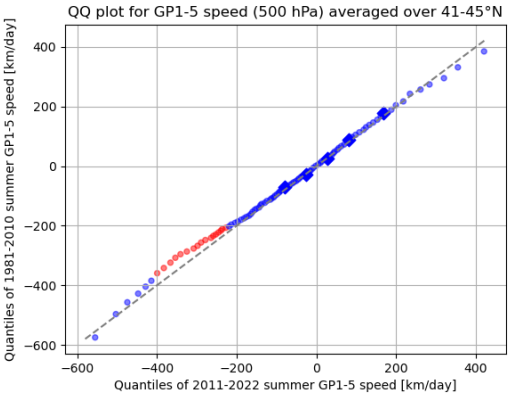

(a) 500 hPa, 41°-45°N

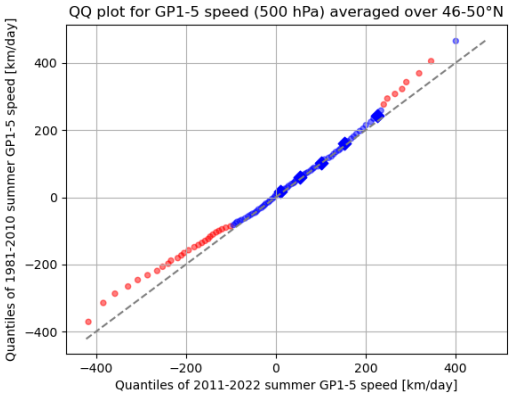

(b) 500 hPa, 46°-50°N

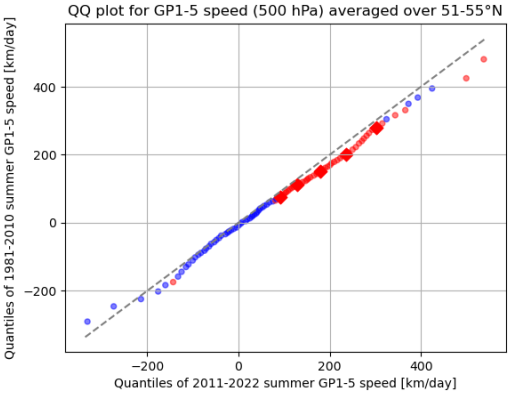

(c) 500 hPa, 51°-55°N

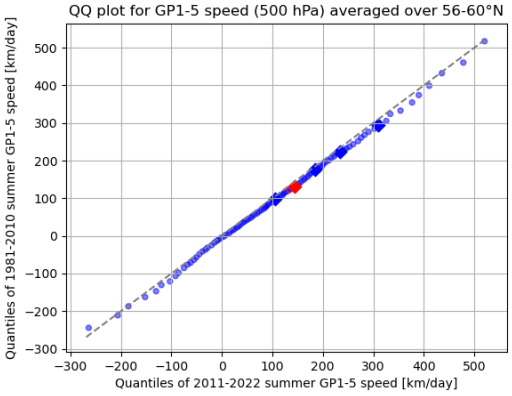

(d) 500 hPa, 56°-60°N

Figure 3.1: QQ plots of GP1–5 speed at 500 hPa for different latitudinal ranges

First, recall that with GP1–5, our main focus is on the potential increase in stationarity of the geopotential height field: the advection of weather systems is related to the propagation of Rossby waves, large meandering anomalies in the geopotential height field, and more stationary Rossby waves are expected to result in more persistent weather with greater, prolonged impact on the surface conditions. The GP1–5 speed can be both eastward (positive) and westward (negative), and therefore a decrease in either of the two tails of the speed distribution implies increased stationarity. Note, however, that due to the negative sign of the westward speed, a decrease in the westward propagation is marked by points lying in the $x > y$ half-plane, unlike the eastward propagation, for which points in that half-plane signalize an increase.

The results show a significant latitudinal dependence. Panels a) and b) in Fig. 3.1 show an increase in the westward propagation, while panel c) shows an increase in the upper half of the eastward propagation speed distribution, suggesting that this part (41°–55°N) of the late-period data distribution is skewed to larger propagation extremes, implying a more frequent occurrence of high-speed days. Only 3.1b) shows a decrease in the eastward propagation speed. The last panel 3.1d) shows that the GP1–5 speed distribution did not undergo almost any significant change in the region from 56°N to 60 °N.

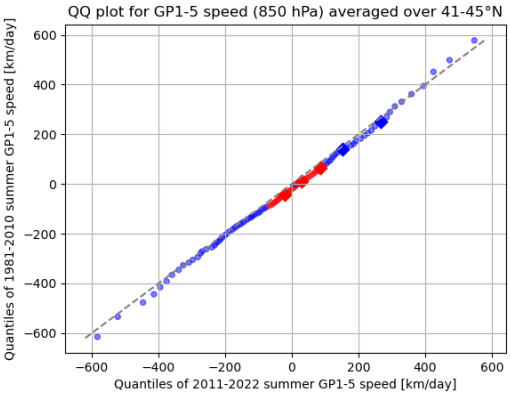

(a) 850 hPa, 41°-45°N

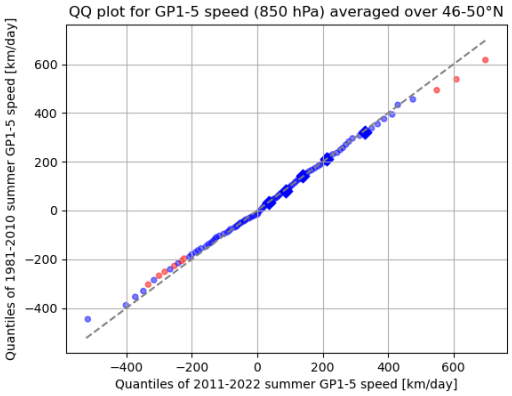

(b) 850 hPa, 46°-50°N

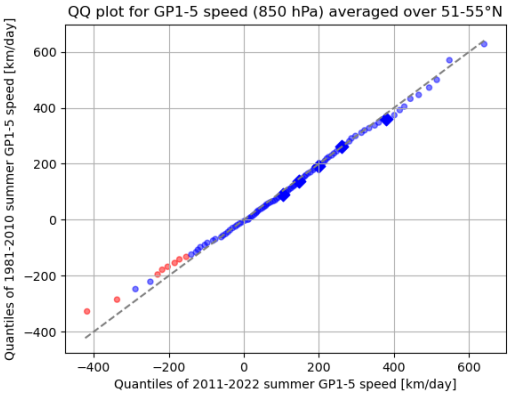

(c) 850 hPa, 51°-55°N

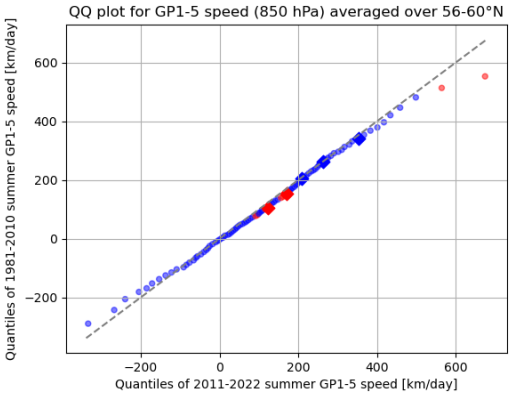

(d) 850 hPa, 56°-60°N

Figure 3.2: QQ plots of GP1–5 speed at 850 hPa for different latitudinal ranges

We provide some help with understanding the QQ plots by relating two of them to the more commonly used histograms and estimates of the probability distribution function. The plots in Fig. 3.3 show how the features visible in the QQ plots translate to the change in the shape of the probability distribution function, which was calculated from the data using Gaussian kernel density estimation. The PDF of the 2011-2022 data in Fig. 3.3a), plotted in red, deviates from the green-plotted PDF of the older data in the same part of the distribution where the points in Fig. 3.1a) divert from the straight line. Similarly, Fig. 3.3b) reflects the increasing trend in the upper half of the probability distribution presented as a QQ plot in Fig. 3.1c).

Figure 3.2 shows the results at the 850 hPa level. Here, the speed variability of GP1–5 between the two observational periods is lower than at the 500 hPa level. Further investigation will be needed to determine whether the changes found at the 500 hPa level in fact did not occur at 850 hPa, or if the peak tracking method is not suitable for use at this lower altitude, given the extent to which the geopotential height field at this level is influenced by perturbations in form of synoptic-scale pressure systems, despite the attempts to filter the noise by the Fourier decomposition.

Due to the large latitudinal variability of the results and the fact that we could not confirm their consistency between the different pressure levels, we conclude that we did not find any overall hemispheric trend in the frequency of occurrence of low-speed summer days.

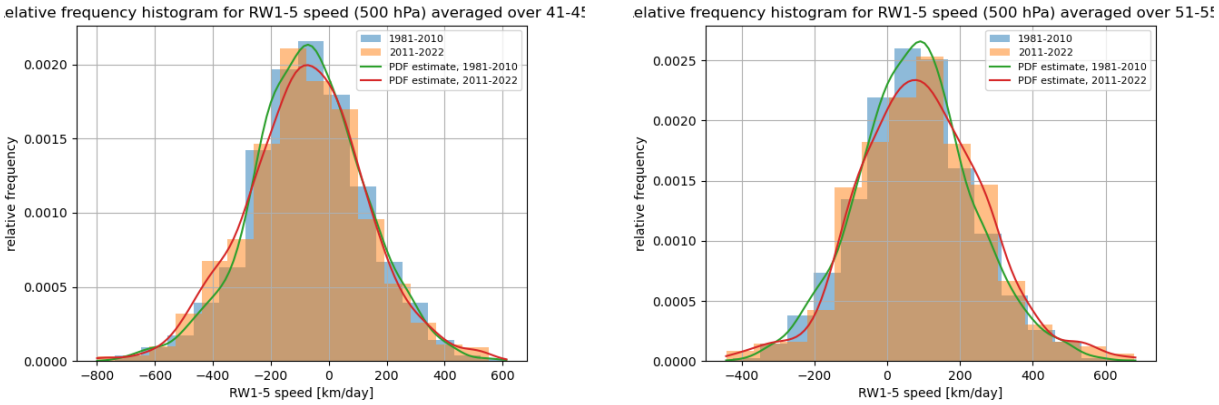

(a) 500 hPa, 41°-45°N

(b) 500 hPa, 51°-55°N

Figure 3.3: Histograms comparing the distributions of the 1981–2010 data and 2011–2022 data. Corresponding probability density functions were calculated using Gaussian kernel density estimation.

This does not necessarily mean that our approach and the peak tracking algorithm are faulty. Our findings are supported by other authors [2] [22], who, using methods based on analyzing high altitude winds instead of geopotential, reported no significant overall decrease in the propagation of Rossby waves during the summer months.

3.1.2 Results of the amplitude analysis

We decomposed the geopotential field into five simple harmonic waves GP1 to GP5 based on the zonal wave number and calculated the corresponding amplitudes. These waves in the geopotential height field can be seen as the manifestation of the long, planetary Rossby waves with zonal wave numbers 1 to 5. As our main focus was the study of summer heatwaves, we assessed changes in the wave amplitude distributions only during the summer months (JJA) by comparing the early-period (1981–2010) and late-period (2010-2022) summer data.

Our overall investigation of the amplitudes of GP1 to GP5 did not, with a few exceptions, yield interesting results. Therefore we do not include them here, in the main text, but we present several selected QQ plots showing the more interesting results in Appendix A.

On the other hand, we found significant trends in the distribution of GP1–5 summer amplitudes. These trends, presented in Figures 3.4 and 3.5, are visible at both pressure levels studied, albeit to a lesser extent at 850 hPa. We report a significant decrease in GP1–5 amplitudes throughout large parts of the mid-latitudes, especially the 46°– 55 °N band. The southernmost region that we studied, 41°– 46 °N, experienced a comparatively smaller decrease at the 500 hPa level, and practically no change at the 850 hPa level. The only region where the results show an increase in the top part of the amplitude distribution is the northernmost region studied, 56°N – 60 °N, at the 850 hPa level. Here, the top ten percentiles show an increase in the occurrence of high-amplitude days, however, in general, a non-significant one.

As much as this sounds contradictory to the earlier presented hypothesis regarding amplitude elongation, it is in line with the findings of its original proponents. In their 2015

article [13], Francis and Vavrus reported an overall hemispheric decrease in the frequency of high-amplitude days during the summer months, while only selected regions experienced the hypothesized increase. Coumou et al. quantified the mean amplitude decrease during summer months as -5% over the period 1979–2013 [9].

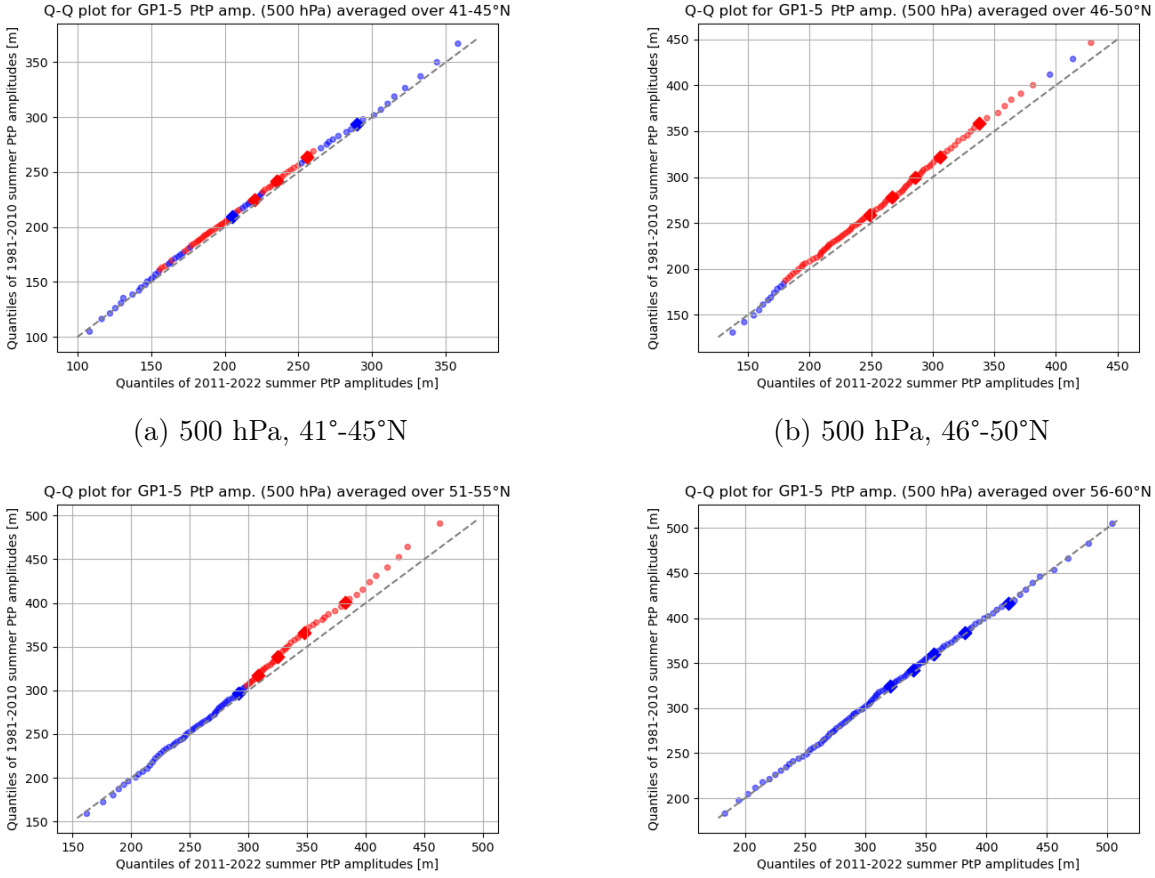

(a) 500 hPa, 41°-45°N

(b) 500 hPa, 46°-50°N

(c) 500 hPa, 51°-55°N

(d) 500 hPa, 56°-60°N

Figure 3.4: QQ plots of GP1–5 peak-to-peak amplitudes at 500 hPa for different latitudinal ranges

3.2 Changes in amplitudes and speed during heatwaves

The main focus of this thesis is to find a correlation between heatwaves, waviness of the geopotential field, and its increased stationarity. Determining whether these phenomena regularly accompany extreme temperature anomalies might be helpful in the prediction thereof, which in turn can help mitigate the damaging impact by providing more time to prepare. It is important to note that we are not able to prove direct causality between heatwaves and anomalous Rossby wave characteristics solely by means of our statistical analysis. To prove such a causal relationship, more conclusive observational and modeling evidence with a solid theoretical background will be needed [1], moreover if we wish to connect the increasing number of heatwaves to Arctic amplification as was previously hypothesized [14]. This task of relating the trends to Arctic amplification is beyond the scope of this thesis.

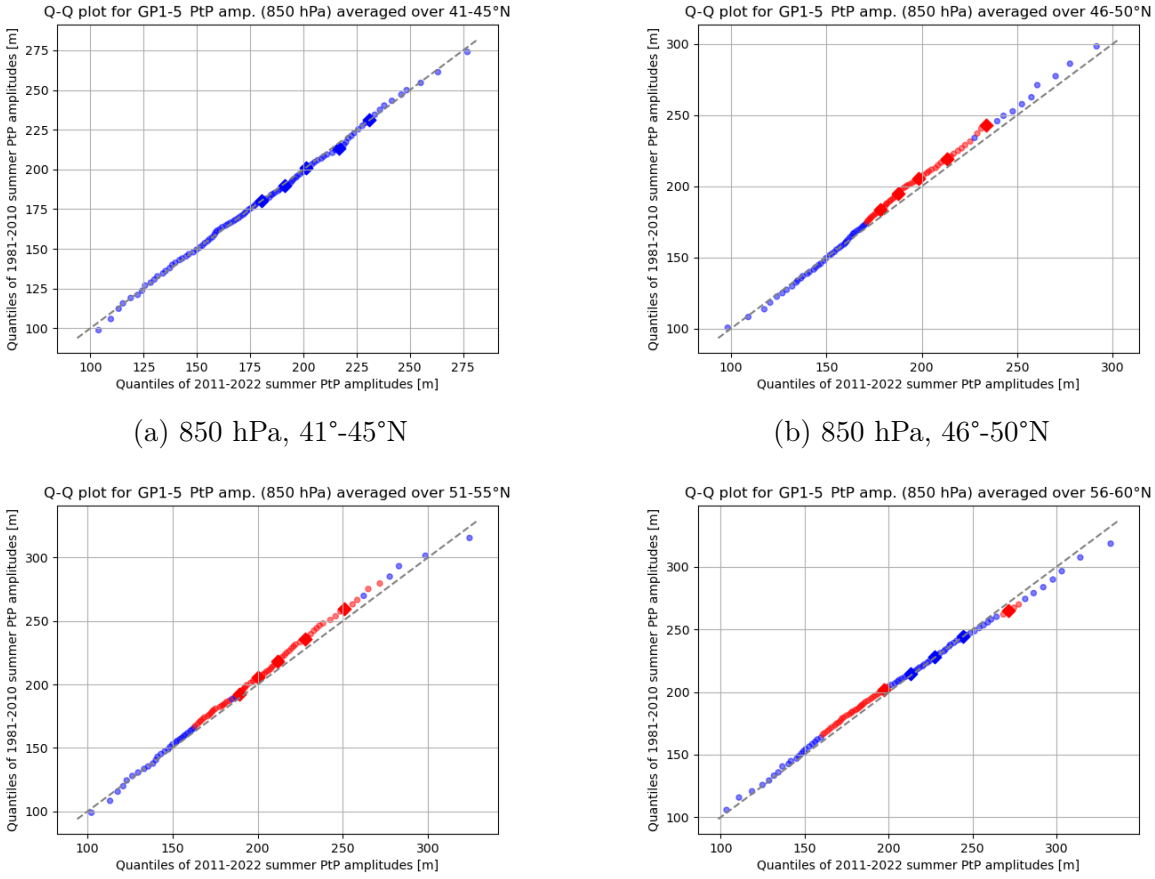

(a) 850 hPa, 41°-45°N

(b) 850 hPa, 46°-50°N

(c) 850 hPa, 51°-55°N

(d) 850 hPa, 56°-60°N

Figure 3.5: QQ plots of GP1–5 peak-to-peak amplitudes at 850 hPa for different latitudinal ranges

To analyze the heatwave-specific patterns in the geopotential field, we needed to create a subset of the geopotential data consisting of days that were determined to be a part of a heatwave using the definition of Russo et al. [23]. We decided to base the data selection on the strongest heatwave that occurred each year within a circle of latitude. At each latitude, we selected the strongest heatwave from each year based on the highest HWMId value, obtaining 44 different heatwaves, one for every year in the period 1979–2022. On average, we selected about 570 heatwave days per latitude, with little difference in this number between southern latitudes and northern ones due to the percentile-based approach to determining heatwaves across regions.

We chose 40°N to 60 °N as the study region for our analysis of anomalous patterns in the geopotential field related to heatwaves. We found the days corresponding to the strongest heatwave around a latitude circle in four different 5-degree-wide latitude bands within the study region. We note that this approach most likely resulted in selecting the same heatwave days more than once at different latitudes since a strong heatwave affects a larger area. However, even by selecting amplitude (speed) data from the same days, but different latitudes, the created dataset will undoubtedly contain heatwave data, and a correctly done significance analysis will yield telling results.

We once again present the results as QQ plots. The significance of the results was determined using a similar Monte Carlo simulation as before, now with heatwave and non-heatwave data selected from the studied latitude band. Then we proceeded as described in the previous section, plotting the results that are significant at the 95% confidence level in red.

3.2.1 Results of the speed analysis

The results of the GP1–5 speed analysis during heatwave days presented in Figs. 3.6 and 3.7 are clearly very different from the previous results regarding the general speed change in the last decade, shown in Figs. 3.1 and 3.2. In the previous section, the results showed a significant latitudinal dependence and were not consistent in the character of the observed changes, with different parts of the mid-latitudes experiencing a positive change in speed, while others saw a negative change or no significant change at all. In addition, no consistency in the changes could be confirmed across different pressure levels.

The results of the heatwave-focused analysis, presented in Figs. 3.6 and 3.7, are more compelling. All four studied latitude bands show a significant decrease during heatwaves in large parts of the GP1–5 speed distribution, especially the positive (eastward) part.

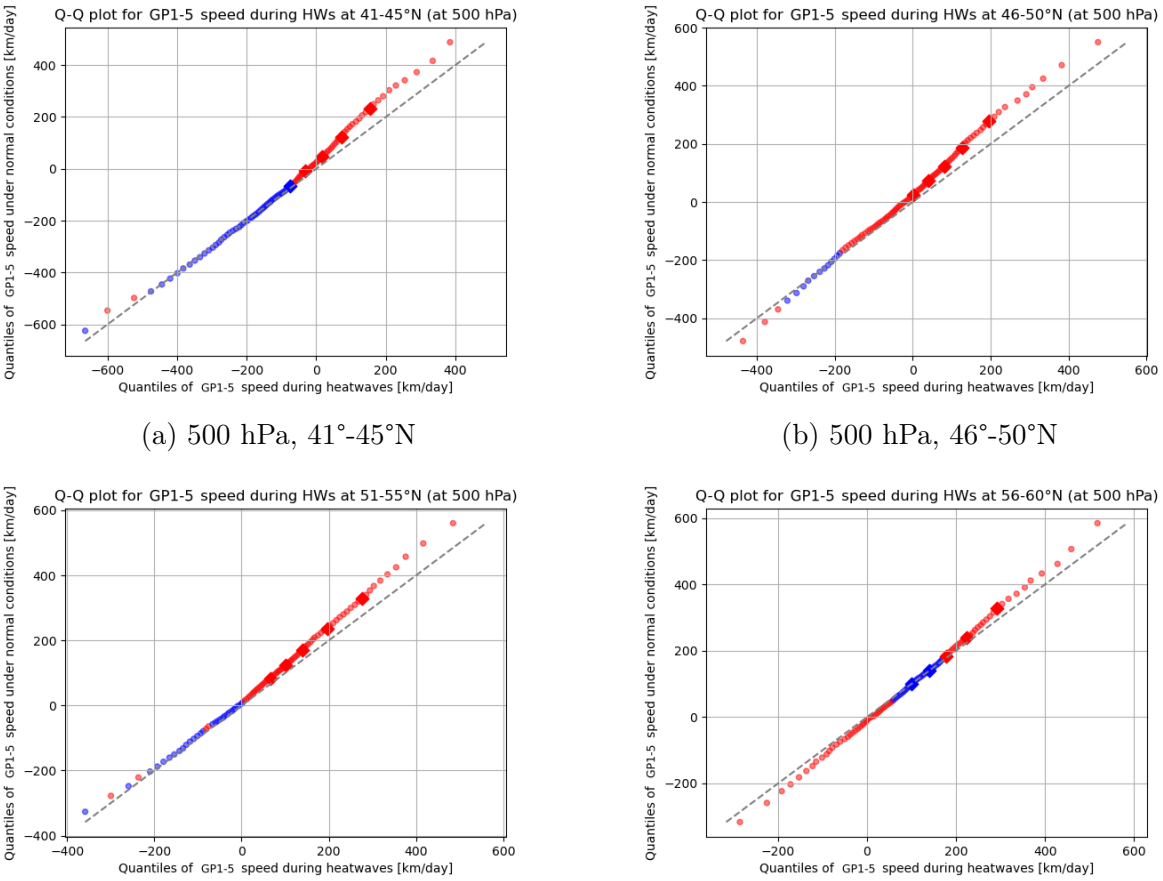

(a) 500 hPa, 41°-45°N

(b) 500 hPa, 46°-50°N

(c) 500 hPa, 51°-55°N

(d) 500 hPa, 56°-60°N

Figure 3.6: QQ plots of GP1–5 speed at 500 hPa for different latitudinal ranges during heatwaves

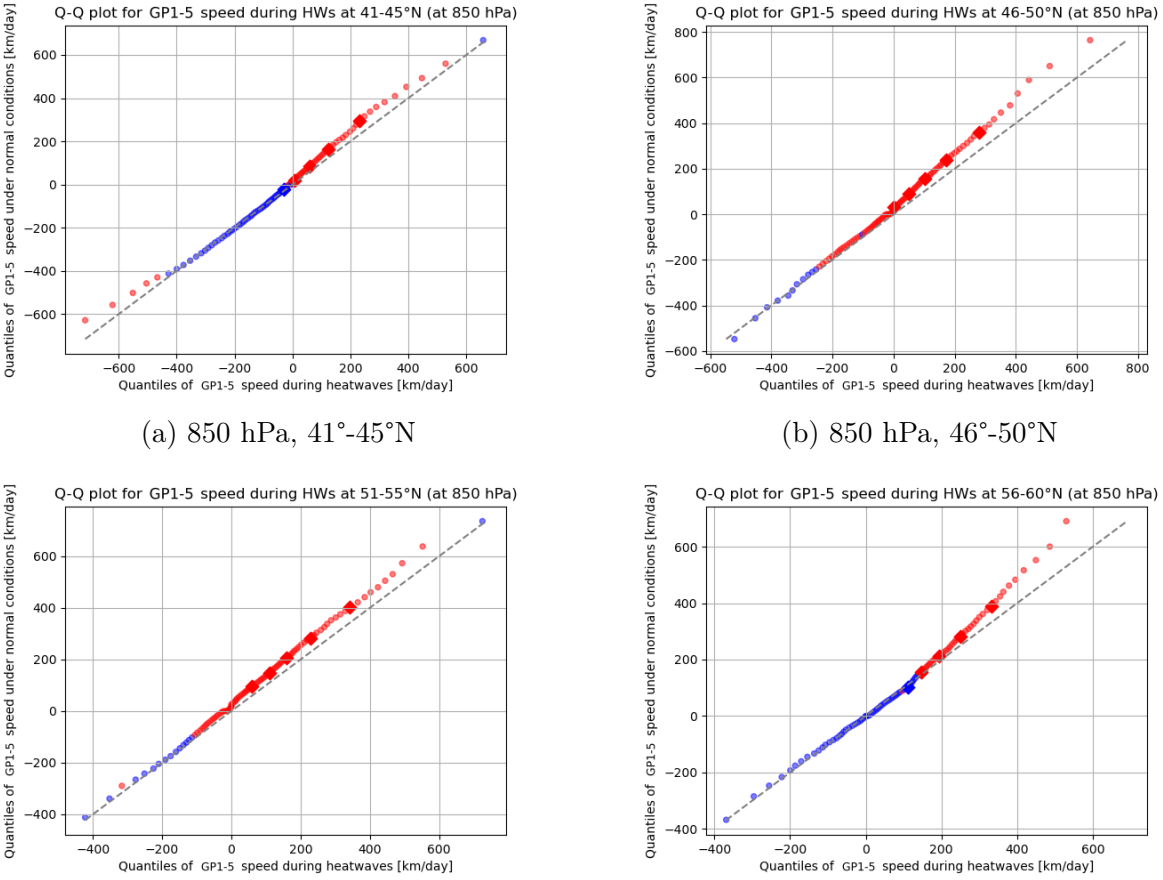

(a) 850 hPa, 41°-45°N

(b) 850 hPa, 46°-50°N

(c) 850 hPa, 51°-55°N

(d) 850 hPa, 56°-60°N

Figure 3.7: QQ plots of GP1–5 speed at 850 hPa for different latitudinal ranges during heatwaves

The same pattern has been observed at both investigated pressure levels. We conclude that there is indeed a significant correlation between slowly eastward-propagating Rossby waves and heatwaves.

It is likely that the peak tracking algorithm identified periods of atmospheric blocking, large-scale stationary patterns in the geopotential field that are often associated with extreme temperature events [17]. Other studies estimated the Rossby wave phase speed using analysis of high-altitude winds and came to the same conclusion, i.e. that the reduced Rossby wave speed systematically accompanies blocking events and temperature extremes [22].

To summarize the changes, we selected the top ten percent of the largest values from both the heatwave and the non-heatwave datasets, calculated the mean difference across the 40°N – 60°N latitude band, and filtered the results using a moving average with a 3-degree-wide averaging window. Figure 3.8 shows the latitudinal changes in the eastward propagation, previously presented in Figs. 3.6 and 3.7, in actual physical quantities, km/day, while the QQ plots show differences in the probability distribution. Notice that the mean difference is negative at all latitudes, proving there has been a consistent, significant decrease in the GP1–5 speed during summer heatwave events.

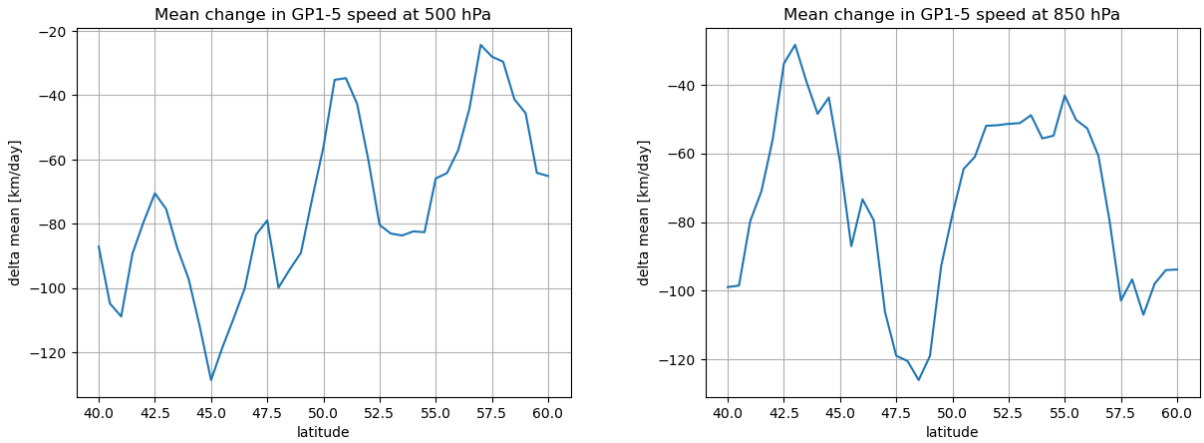

(a) 500 hPa (b) 850 hPa

Figure 3.8: Mean difference between GP1-5 speed during heatwave periods and non-heatwave periods, expressed in km/day.

Further research is needed to determine whether such periods with low wave speed are becoming more frequent, as our previous results did not show a significant hemispheric trend. However, regional trends were found, and therefore focusing on a specific region that has experienced an increased number of heatwaves might yield a more conclusive outcome. An additional review of the used method and further examination of the subject, possibly in a narrower spatial region, is necessary.

3.2.2 Results of the amplitude analysis

The results of the amplitude analysis in the context of summer heatwaves, presented in Figs. 3.9 and 3.10, show significant changes in all studied latitudinal bands. In three of the four regions, nearly the whole amplitude distribution during heatwaves is skewed relative to the non-heatwave conditions, but the character of the changes varies. In the southern parts of the studied region, 41°– 50°N, the amplitudes tend to be lower during heatwaves compared to normal conditions. Approaching more northern latitudes, the trend reverses, and the amplitudes tend to increase during heatwaves. Virtually the same differences were observed at both investigated pressure levels.

Based on Figs. 3.9 and 3.10, the average shift of the distribution from lower to higher amplitudes is continuous in the meridional direction. The summarizing Fig. 3.11 shows the mean difference between the top ten percentiles of the heatwave and the non-heatwave distributions latitude by latitude, assigning physical units to the observed changes.

Francis and Vavrus argued that high-amplitude waves progress slower and therefore increase the probability of an extreme event by making the associated weather patterns more persistent [14]. The authors base this claim on theoretical arguments, but we were able to find observational evidence supporting this mechanism. While we did confirm that the propagation speed of high-amplitude waves tends to be reduced (results shown in Appendix B) compared to lower-amplitude waves, our analysis only showed an amplitude increase in the 50°–60°N latitude band, whereas the amplitudes in the southern part of the studied region, 41°– 50°N, showed a significant decrease during heatwaves. This

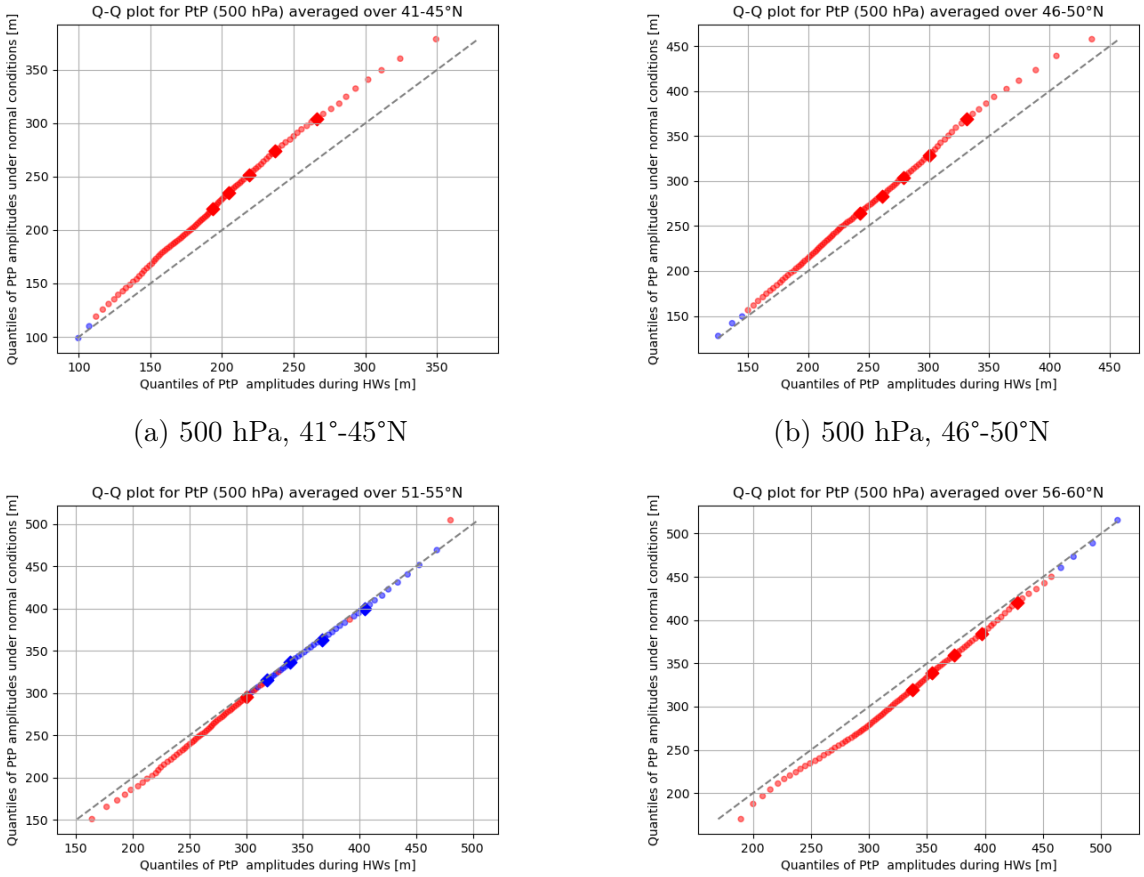

(a) 500 hPa, 41°-45°N

(b) 500 hPa, 46°-50°N

(c) 500 hPa, 51°-55°N

(d) 500 hPa, 56°-60°N

Figure 3.9: QQ plots of GP1–5 peak-to-peak amplitudes at 500 hPa for different latitudinal ranges during heatwaves.

suggests that the heatwave-causing mechanisms are more complex and possibly latitude-dependent.

We propose a hypothesis, that heatwaves in the southern mid-latitudes are associated with low-amplitude settings that favor zonal flow and thus reduce heat exchange and cold air advection from the north, whereas the heatwaves in the northern mid-latitudes are more frequently accompanied by high-amplitude waves, that conversely enhance energy transport into the region. Zschenderlein et al. reported similar patterns in the 500 hPa geopotential field associated with European heatwaves [32]. We expand on their results by confirming that this trend can be observed in the whole 40°–60°N latitude band. As this is perhaps the most interesting result of this thesis, it will be discussed more thoroughly later on.

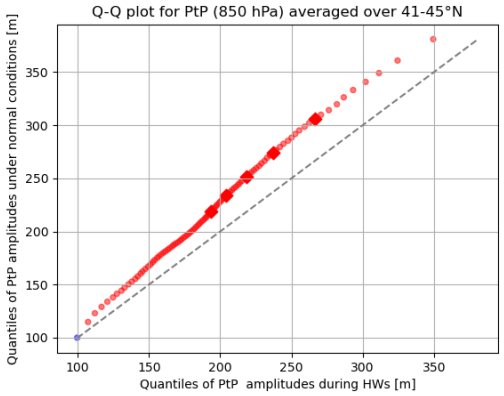

(a) 850 hPa, 41°-45°N

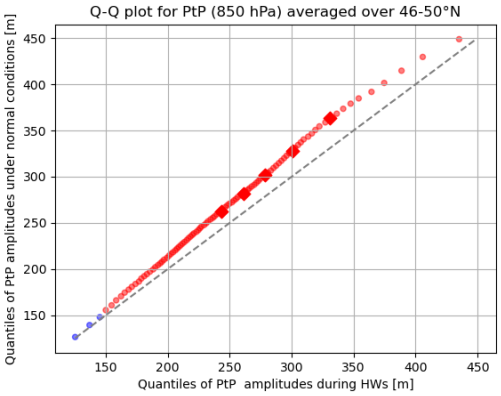

(b) 850 hPa, 46°-50°N

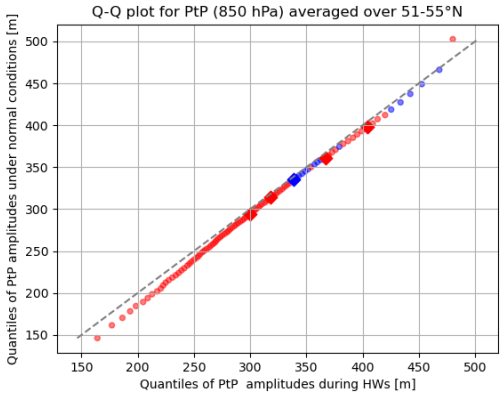

(c) 850 hPa, 51°-55°N

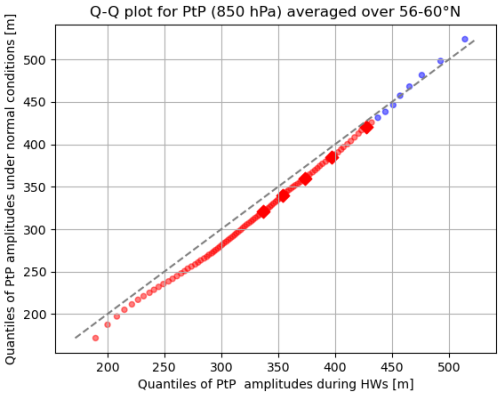

(d) 850 hPa, 56°-60°N

Figure 3.10: QQ plots of GP1–5 peak-to-peak amplitudes at 850 hPa for different latitudinal ranges during heatwaves.

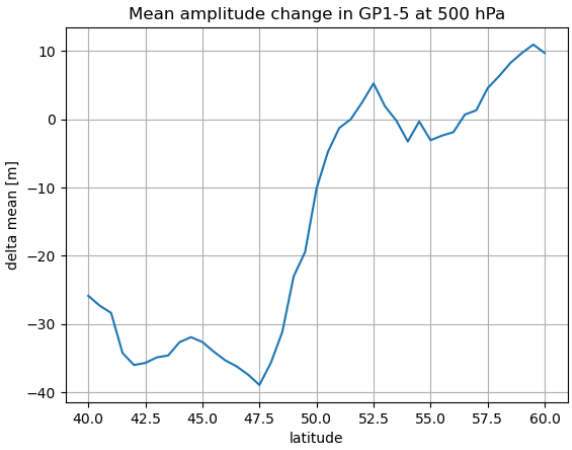

(a) 500 hPa

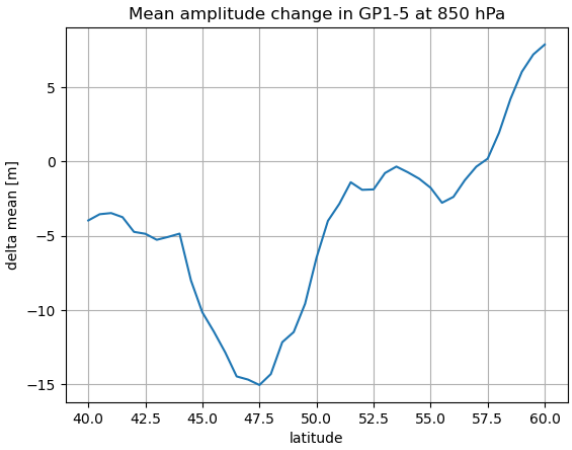

(b) 850 hPa

Figure 3.11: Mean difference between GP1-5 peak-to-peak amplitudes during the heatwave periods and outside of the heatwave periods, expressed in meters.

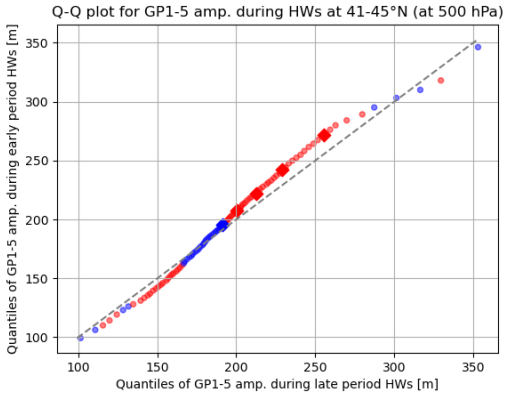

(a) 500 hPa, 41°-45°N

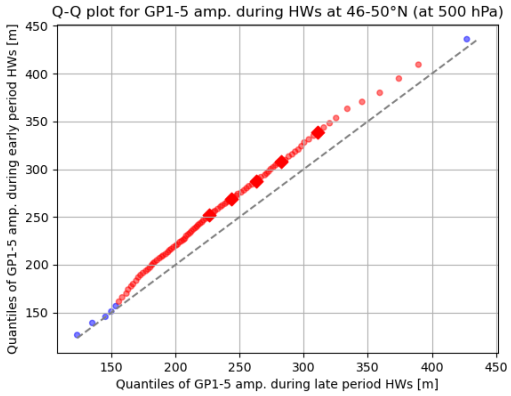

(b) 500 hPa, 46°-50°N

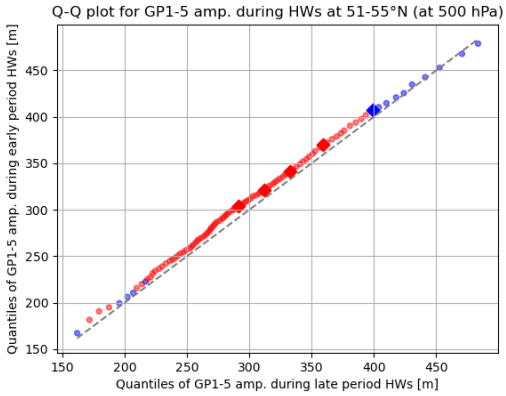

(c) 500 hPa, 51°-55°N

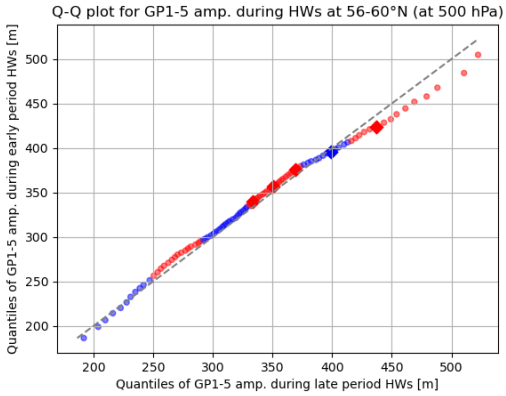

(d) 500 hPa, 56°-60°N

Figure 3.12: QQ plots of GP1–5 peak-to-peak amplitudes at 500 hPa for different latitudinal ranges during early-period (1979–2010) and late-period heatwaves (2011-2022).

3.2.3 Early-period and late-period heatwaves

We investigated the changes in the wave speed and amplitudes only during heatwave days by splitting the heatwave dataset into two parts: early-period heatwaves, occurring between 1979 and 2010, and late-period heatwaves from 2011–2022. This way, we could assess the tendencies in wave characteristics that systematically coincide with heatwaves, and identify whether the potential heatwave-causing mechanisms have changed over time. We only present the results of the amplitude analysis in the main text (Figs. 3.12 and 3.13), but include the speed results in Appendix C.

The results show that the GP1–5 amplitude tendency is decreasing in the south and increasing in the north when comparing the early-period and late-period heatwaves, primarily at the 500 hPa level. This indicates that there have been changes in the heatwave-causing mechanisms related to atmospheric circulation and Rossby waves, and the results therefore further support the earlier proposed hypothesis about the latitude-dependent character of these mechanisms.

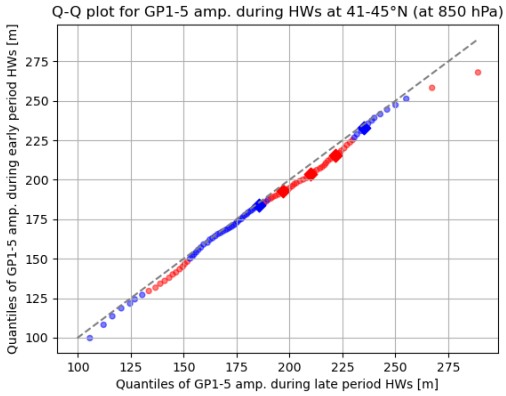

(a) 850 hPa, 41°-45°N

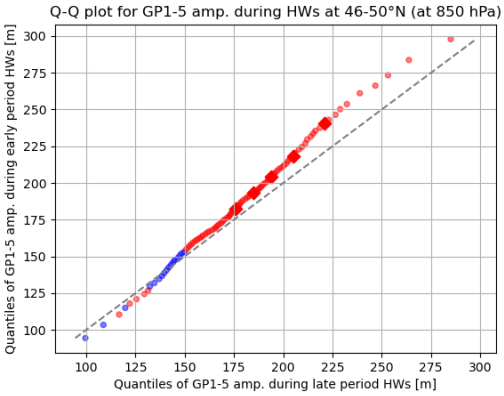

(b) 850 hPa, 46°-50°N

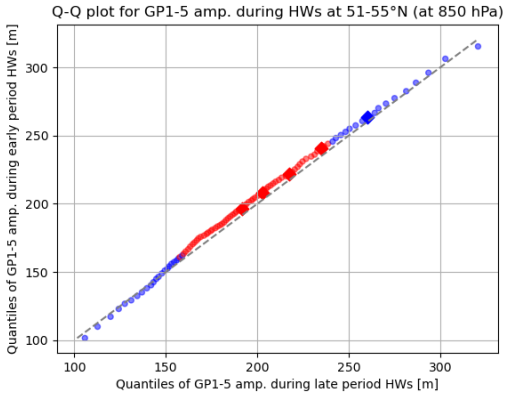

(c) 850 hPa, 51°-55°N

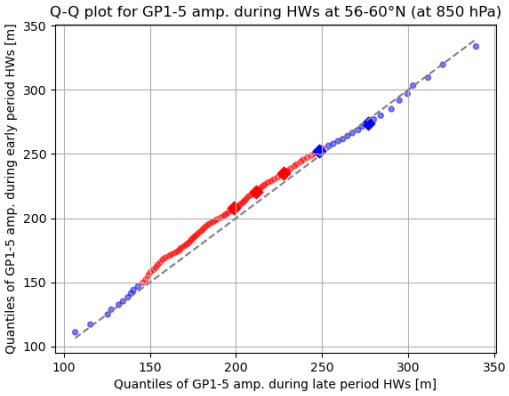

(d) 850 hPa, 56°-60°N

Figure 3.13: QQ plots of GP1–5 peak-to-peak amplitudes at 850 hPa for different latitudinal ranges during early-period (1979–2010) and late-period heatwaves (2011-2022).

Chapter 4

Discussion and conclusion

In this thesis, we used ERA5 reanalysis data to investigate several research questions. First, we focused on the general characteristics of the planetary Rossby waves, and we carried out a statistical analysis examining the trends in propagation speed and amplitudes during the summer months. Next, we selected the strongest heatwaves of the last 44 years and tried to identify any discernible patterns in the characteristics of Rossby waves that correlate with extreme temperature events.

We now further interpret the results and review the methods used during the analysis and compare them to those other authors used in their studies. By identifying the strengths and weaknesses of our methodological choices, we can present the limitations of our results more accurately. We suggest improvements that can help move forward the research in this area.

4.1 Results interpretation

The results do not show any consistent hemispheric trends in the overall propagation speed of Rossby waves during the summer months. A possible explanation could point back to Arctic amplification: the summer has seen the least Arctic amplification from all seasons (see Fig. 1.1). Therefore the meridional temperature gradient is least affected during the summer months, leaving the zonal winds nearly unaltered, based on the simple reasoning using the thermal wind relation (1.2).

Although no overall hemispheric trend could be established, we found significant variations in the individual latitudinal bands. Furthermore, the results presented in Appendix B, stating that higher amplitude waves are associated with lower propagation speed and vice versa, serve as a link between the results regarding the regional tendencies in amplitudes and speed. Notice the nearly one-to-one correspondence between the regional speed trends (Fig. 3.1) and the corresponding amplitude trends (Fig. 3.4) at 500 hPa. The regions which in general experienced a significant increasing trend in GP1–5 speed also experienced a decrease in the amplitude distribution. Conversely, the northernmost studied region, 56°–60°N, where the speed distribution remained unchanged between the two investigated

periods, shows no change in the amplitude distribution. This observed connection gives further credibility to the used methods.

Next, we present our hypothesis on how the general amplitude trends can be related to heatwaves in different latitudinal bands. As can be seen in Figs. 3.9 and 3.10, heatwaves in the southernmost studied region are associated with lower amplitude waves in the geopotential field, whereas heatwaves in the northernmost region are associated with large amplitude waves. In the south, this leads to a more zonal flow, and therefore reduced heat exchange and reduced advection of cold air from the north. In the north, the elongated Rossby waves enhance energy transport into the region and cause the advection of warmer air masses from the south. At the same time, Figs. 3.6 and 3.7 show that heatwaves are associated with reduced propagation speed regardless of the region, thus making the patterns in the geopotential field longer-lasting, boosting their effects on the surface conditions.

Similar results regarding the patterns in the 500 hPa geopotential height field were previously reported by Zschenderlein et al. [32] for European heatwaves. The authors analyzed heatwaves in several European regions, and by plotting composites of the 500 hPa geopotential, made by averaging over all the extreme events within a region, they found large differences in the wave patterns, namely that heatwaves in Scandinavia are in general associated with a high-amplitude, omega-like blocking structure, whereas heatwaves in Southern Europe occur during periods with relatively non-disrupted zonal flow associated with low amplitudes. Our findings confirm their results, while also stating that this setting is true for all heatwaves in the 40°–60°N latitude band, regardless of the specifics of the European climate.

These findings are further supported by the results shown in Fig. 3.12. Compared to heatwaves that occurred from 1979 to 2011, the recent heatwaves (2011-2022) are more often associated with decreased Rossby wave amplitudes in the south and increased amplitudes in the north. These changes are, however, similar to the general amplitude trends found in the individual latitude bands (Figs. 3.9 and 3.10). This indicates, together with the previously proposed hypothesis, that a part of the observed increase in the number of temperature extremes can possibly be attributed to changes in the atmospheric dynamics that might yet not be fully visible in the entire data distribution, but which have already strongly manifested themselves in the formation of heatwaves. Based on our hypothesis, if the current amplitude trends continue and possibly strengthen, we can expect an increase in heatwave activity.

4.2 Different methodological approaches

4.2.1 Identifying Rossby wave characteristics

The methods used by Francis and Vavrus [14] [13] were questioned on the basis of sensitivity to the parameters that the authors decided to use. Their analysis of the wave amplitudes was based on seasonal meridional excursions of selected contours of 500 hPa geopotential height. While they claimed that their selection of contours is representative of the Rossby wave pattern and coincides with the streamline of the strongest 500 hPa winds, their methods were challenged and the results were labeled as non-robust. Barnes

showed that by choosing a wider range of geopotential isolines and by defining the wave on a daily time scale, instead of a seasonal one, as done by Francis and Vavrus, one can report contradictory trends in the wave amplitudes [2]. She identified the flaw in their methods to be the specific choice of analysis parameters, i.e. the specific geopotential height contours used to describe the wave amplitude.

This is an example of how the robustness of reported results can depend on parameters, whose choice, albeit well thought out, is to a certain extent still *ad hoc*. It is important to test the significance of any findings by varying these free-to-choose parameters and seeing how the results are influenced by them.

Our approach to analyzing the waviness of the geopotential field and its zonal progression is based on a Fourier decomposition of the field on two pressure levels, 500 hPa and 850 hPa. Most of the analysis was carried out using GP1–5, an approximation of the field created by truncating the Fourier series after five terms. The metric used for determining waviness was the peak-to-peak amplitude, the difference between the highest ridge and the lowest trough on a given day around a circle of latitude. We consider the low number of arbitrary analysis parameters to be one of the main strengths of our approach to studying the trends in wave amplitudes. The choice of GP1–5 as the representative approximation of the geopotential field was motivated by the need to separate the long, planetary Rossby waves from smaller-scale features of the atmospheric flow. Nevertheless, to test the results, the same analysis should be carried out with a GP approximation composed of a different number of waves, and possibly on more pressure levels to investigate the consistency of the trends across different altitudes.

The propagation speed of GP1–5 was estimated using a peak-tracking algorithm that we developed, and it contains several parameters which were determined predominantly based on physical intuition. We estimated the speed by following the movement of peaks of GP1–5 within a 25-degree-wide region on seven consecutive days. The width of the region was decided based on the assumption of continuous changes in the geopotential field on a daily time scale. The length of the tracking period, one week, was chosen based on the average lifespan of a weather system, one that might possibly cause a temperature extreme. The sensitivity of the reported results to these parameters of the tracking algorithm was not examined.

We should note that the methods we described here are not the only methods that were tested. At first, we attempted a case study, where we selected several heatwave events and investigated the properties of the individual GP waves as well as of the sum thereof, and we searched for any commonalities in the wave characteristics between these events. We tried estimating the propagation speed of GP1–5 using cross-correlation, a method commonly used in signal processing to estimate the similarity of two wave signals, but we found the method to be not sensitive enough for the day-to-day changes in the geopotential field. Overall, the results of the case study were not satisfactory, and therefore we resorted to the statistical analysis presented here, which appeared to be a more promising approach.

4.2.2 Heat wave selection

There is no uniform definition of a heatwave. There is however a general understanding of what a heatwave is, i.e. a period with abnormally high temperatures, and indeed, some authors used this simple notion to come up with indices for classifying heatwave mag-

nitude, identifying heatwaves as a period of days with temperatures reaching 5° above climatology [24]. But this threshold is too high for climate regions with a low temperature variability, namely the tropics, and such a definition thus makes the comparison of individual heatwaves across regions difficult. To overcome this obstacle, Russo et al. proposed HWMId, the heatwave magnitude index daily, a percentile-based heatwave index that is applicable to various climate regions thanks to its reference to local climatology and the local temperature trends [23].

We identified all instances of heatwaves in each gridpoint of the dataset. However, later in our analysis, we only considered the strongest heatwave that occurred each year, as determined by the highest HWMId value. This choice made the analysis easier to perform, but it also artificially reduced the sample size, possibly by as much as half, based on the knowledge that during a typical summer in the Northern Hemisphere, one or two heatwaves occur [32]. We partially overcame the issue by selecting values from a wider range of latitudes, thus increasing the sample size of heatwave data. Nevertheless, we acknowledge the limitations of our approach. For future research, we suggest focusing on smaller spatial regions, which will make the results more relevant to the given location, accurately describing the local working mechanisms. It will also make the analysis more computationally feasible.

4.3 Future research

The analysis possibilities of our datasets and the potential of our methods have not been fully exhausted. There are several questions that should be answered to further investigate the diverse nature of heatwave-causing mechanisms. Are specifically the recent large-amplitude waves slowing down relative to the early period large-amplitude waves? According to our hypothesis, this would lead to more temperature extremes in the northern mid-latitudes. What is the amplitude trend of the slow-moving waves? An increasing amplitude trend would favor heatwaves in the north, whereas a decreasing trend would favor heatwaves in the south.

It has been suggested that other types of extreme events are also affected by trends in the dynamical properties of atmospheric circulation. Our methods can be used to examine the influence that the Rossby waves have on cold spells and extreme precipitation events. Based on previous research, we expect to see larger changes in the wave properties during seasons other than summer, owing to the seasonal differences in Arctic amplification, which is the strongest during the cold months of the year. Therefore investigating these ongoing changes and finding out more about their correlation with other types of extreme events might reveal more about the nature of extreme events in the future climate.

Using a method developed by Graversen and Burtu [15], heat transport and the associated energy convergence and divergence can be studied, helping to understand the relationship between atmospheric circulation and extreme events. Their method, similar to our approach, is based on a Fourier decomposition of the energy transport with respect to the zonal wave numbers, and therefore it can be applied as a natural extension of our analysis. By decomposing the energy transport and focusing on the part associated with the planetary Rossby waves, it can be determined how much energy is brought into a

region by the waves, and thus decided whether an extreme event is directly related to advection of air masses.

Modeling studies can be conducted to truly investigate the causal relationship between Arctic amplification and Rossby waves, and between Rossby waves and extreme events. By changing the magnitude of Arctic amplification, and by reinforcing conditions that lead to a more stationary zonal flow, we could learn about the inner working mechanisms that augment the frequency of extreme weather events.

4.4 Conclusion

Recent years have witnessed a rising trend in heatwave activity. With this increase comes a question: have the heatwave-causing mechanisms changed? While it is virtually certain that the continuing global warming directly impacts the frequency and severity of heatwaves through the rising average temperature, there are possibly other, less obvious warming-related effects, whose influence should not be underestimated if we wish to fully understand the ongoing changes in the Earth's climate system.

This thesis focused on the linkage between heatwaves in the mid-latitudes and upper-level atmospheric circulation during the summer months. We investigated the circulation hypothesis, proposed by Francis and Vavrus in 2012 [14], which relates trends in the properties of Rossby waves to extreme events. The authors argue that these changes are induced by Arctic amplification, the uneven nature of global warming, which is accelerated in the Arctic regions compared to the rest of the Northern Hemisphere. We did not attempt to verify this part of the hypothesis, however, by means of statistical analysis, we examined whether the propagation speed of the waves and their amplitudes in recent years are subjected to change. We further looked for links between the changes and extreme temperature events.

Using an approach based on Fourier decomposition of the geopotential field, we separated the large-scale planetary Rossby waves from the synoptic-scale waves, calculated amplitudes of the geopotential anomalies, and estimated the wave speed using a newly developed peak-tracking algorithm. After establishing a daily time series of amplitudes and wave speeds for the period 1979–2022 (JJA), we carried out an analysis of the underlying trends. Next, a subset of the time series was selected, based on days that were identified as being a part of a heatwave. HWMId, a percentile-based index proposed by Russo et al. [23] was used in the identification of heatwave events.

The heatwave-related results lead us to formulate a hypothesis regarding latitudinal variations in the heatwave-causing mechanism. We found that while the Rossby wave speed tends to be slower during heatwaves across all latitudes, the trends in their amplitudes differ: in the southern mid-latitudes, heatwaves are associated with lower-amplitude circulation patterns, whereas in the north, heatwaves are more often accompanied by high-amplitude Rossby waves.

By comparing heatwaves from two different time periods, 1979–2010 and 2011–2022, we found that the recent heatwaves occurring in the north are more often associated with the aforementioned high-amplitude setting than they were in the early period. The same trend, but with low-amplitude waves, was found in the southern latitudes. These results

indicate that the trends in atmospheric circulation are part of a heatwave-inducing mechanism that acts on top of the observed global temperature increase and possibly causes extreme events with stronger harmful impacts.

While we could not confirm any overall hemispheric tendencies in either Rossby wave propagation speed or their amplitudes during the summer months, we found significant regional trends in the wave amplitudes that could be observed at both studied pressure levels. Contrary to the basic premise of the circulation hypothesis, the trend was decreasing in most of the latitude bands that we studied. Through our hypothesis, this could relate to an increased heatwave activity in the lower mid-latitudes. We further confirmed that high-amplitude waves are characterized by reduced propagation speed, a claim found in previous studies that was based on theoretical arguments, but with little observational evidence. Finally, the results found regarding the overall trends in the wave propagation speed were inconclusive.

The rate at which the Earth is warming is increasing with every decade, and despite all warnings, we are still far from the 1.5-degree pathway. We may not succeed in the mitigation of global warming. However, by knowing more about extreme events, we can be better prepared for what the future holds. Infrastructure investments, abandoning water-intensive agriculture, and creating heat preparedness plans with disadvantaged regions in mind, these are the measures necessary to diminish the concerning prospects of future extreme events.

Appendix A

Trends in GP amplitudes

We first decomposed the geopotential field in its fundamental harmonic components GP1 to GP5. The first five terms of the Fourier series can be interpreted as the manifestation of the long Rossby waves with zonal wave numbers 1 to 5 in the geopotential field. Since GP1–5 is the sum of GP1 to GP5, it makes sense that the trends in GP1–5 are tightly connected to the trends in the individual waves. Here we present only the extreme cases.

The largest changes contributing to the trends in GP1–5 were observed in GP3 on both 500 hPa (Figure A.1) and 850 hPa levels (not shown). On the other hand, GP2 did not contribute to the decrease in GP1–5. Its top percentiles even experienced an increase in the northernmost parts of the studied region, which was largely counteracted by the behavior of the other waves (Figure A.2).

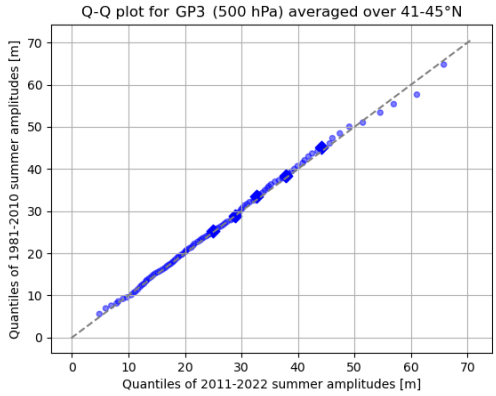

(a) 500 hPa, 41°-45°N

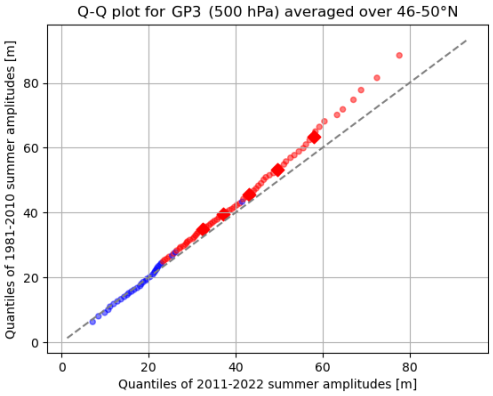

(b) 500 hPa, 46°-50°N

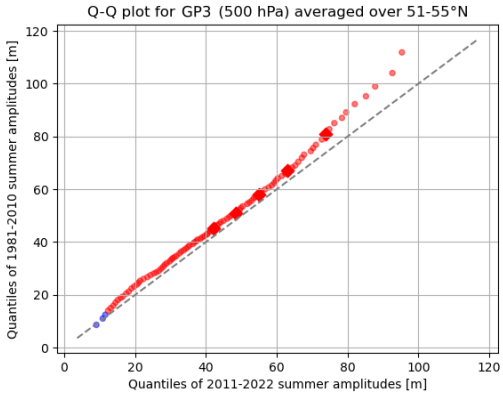

(c) 500 hPa, 51°-55°N

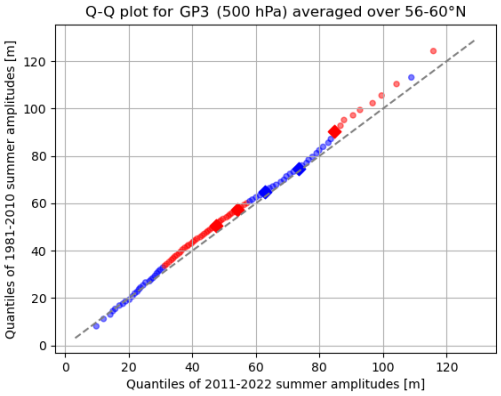

(d) 500 hPa, 56°-60°N

Figure A.1: GP3 amplitudes at 500 hPa show the most pronounced changes from all individual waves.

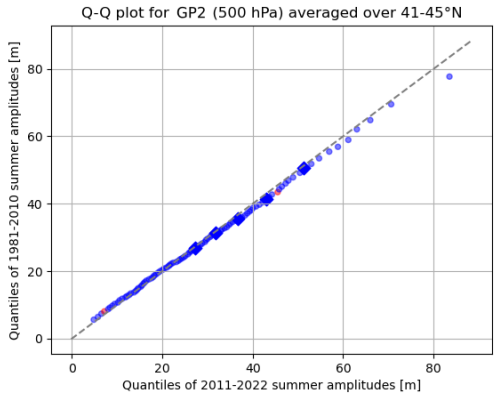

(a) 500 hPa, 41°-45°N

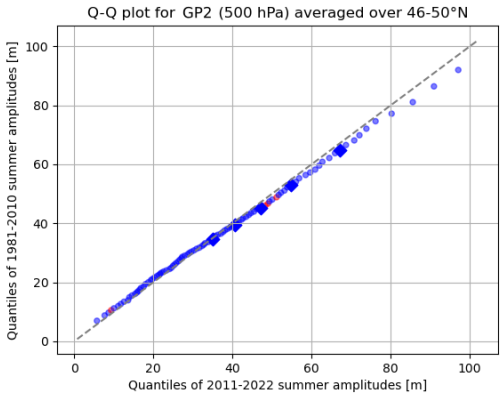

(b) 500 hPa, 46°-50°N

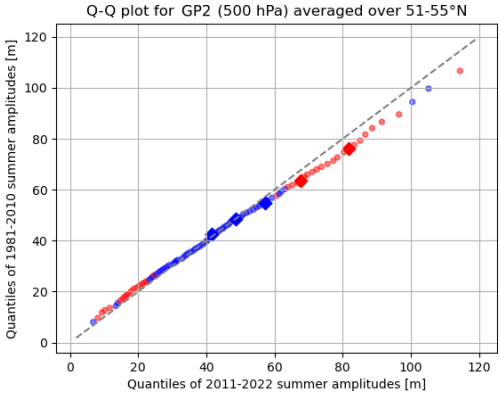

(c) 500 hPa, 51°-55°N

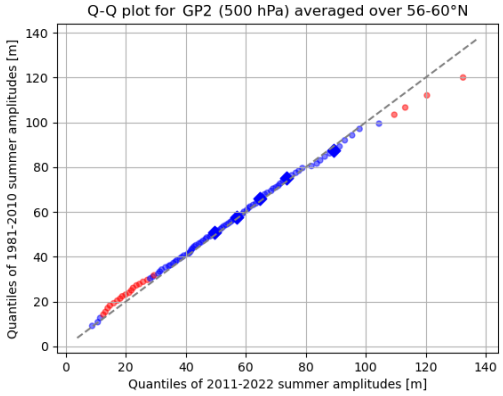

(d) 500 hPa, 56°-60°N

Figure A.2: GP2 amplitude at 500 hPa showing an opposite trend to GP1–5.

Appendix B

Propagation speed of high-amplitude waves

In their original article, Francis and Vavrus mention a relationship between high-amplitude Rossby waves and decreased propagation speed [14]. To test this, we selected the waves with amplitudes in the top 25% of the distribution and studied their propagation speed in contrast to the speed of the lower-amplitude waves. We confirmed that high-amplitude waves propagate slower, and this trend is significant in both the eastward and the westward propagation (less so at the 850 hPa level). If the hypothesized increasing trend in Rossby wave amplitudes is ever confirmed, we can expect a reduction in the speed of the atmospheric flow, which in turn correlates with heatwaves, as we have shown before.

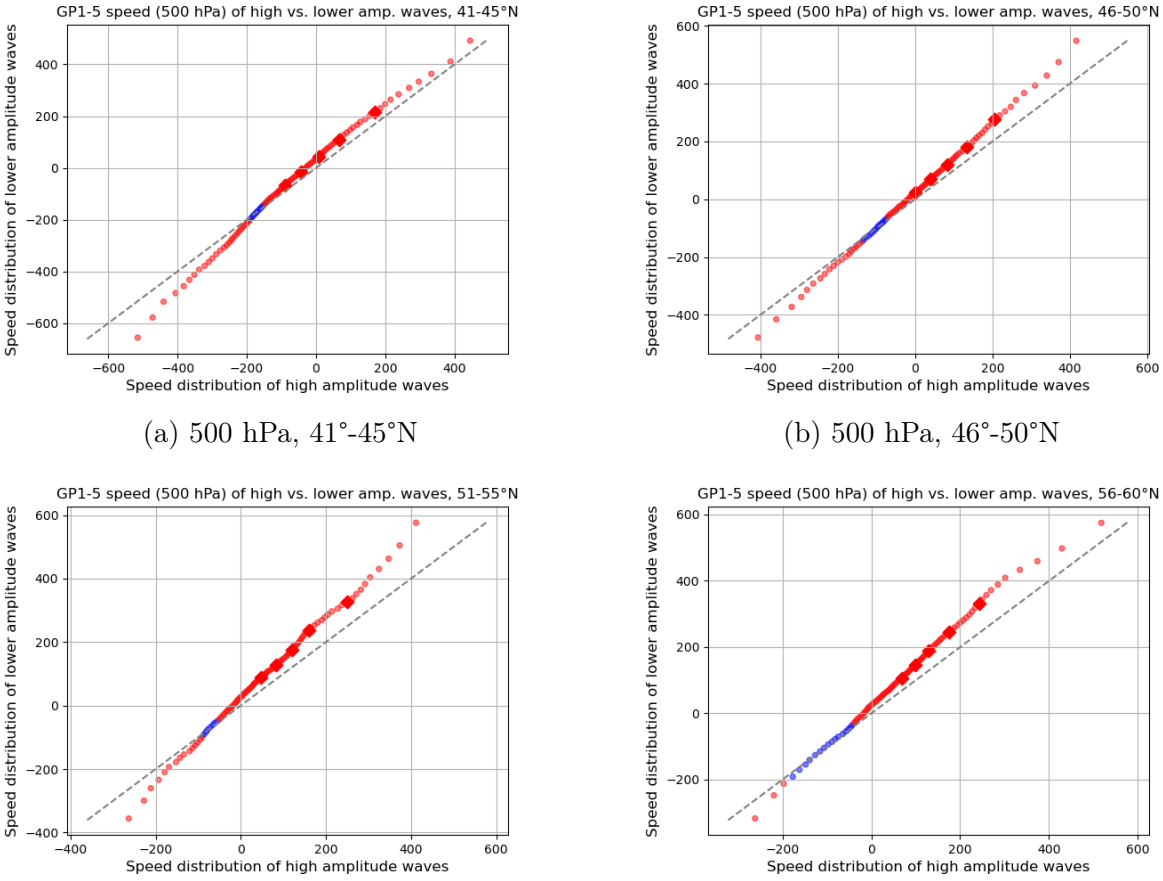

(a) 500 hPa, 41°-45°N

(b) 500 hPa, 46°-50°N

(c) 500 hPa, 51°-55°N

(d) 500 hPa, 56°-60°N

Figure B.1: Comparison of the speed distributions of high-amplitude and lower-amplitude waves at 500 hPa. Notice the differences are highly visible in both tails, showing that both westward and eastward propagation is affected.

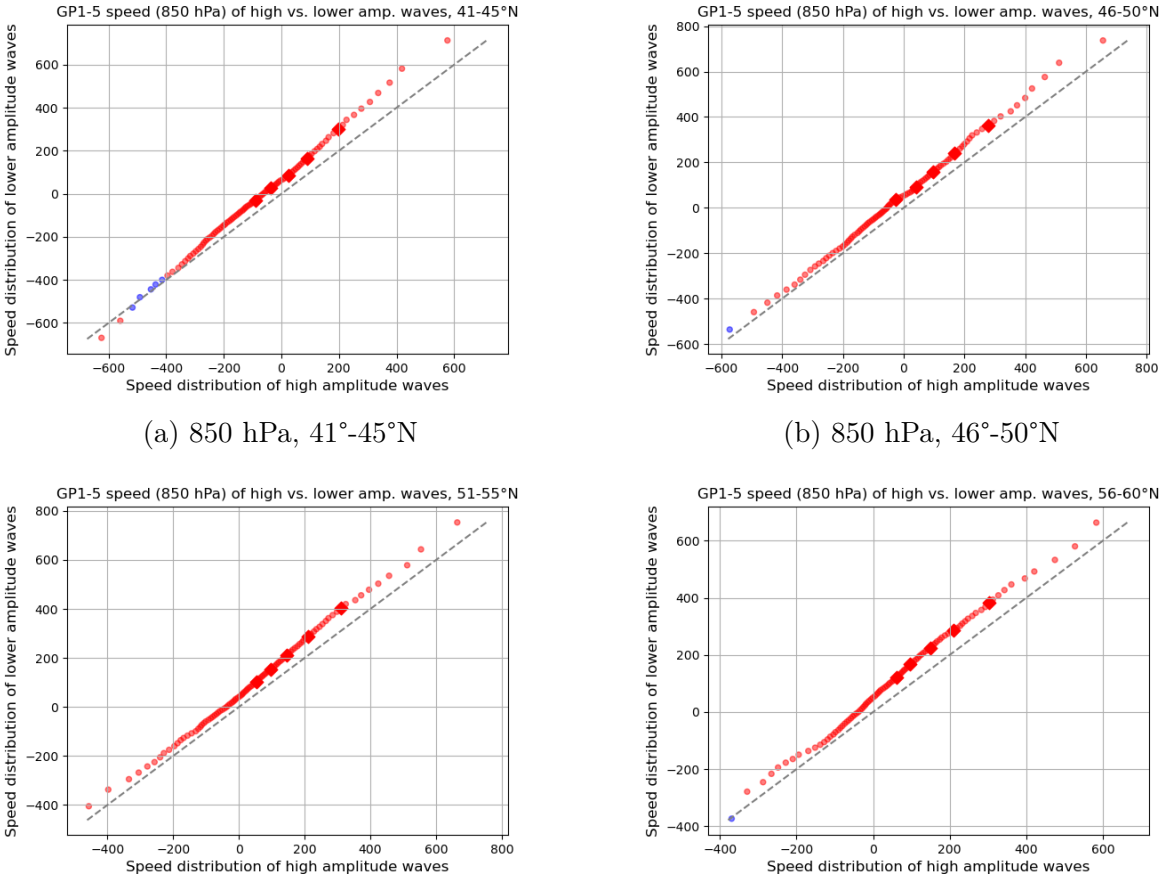

(a) 850 hPa, 41°-45°N

(b) 850 hPa, 46°-50°N

(c) 500 hPa, 51°-55°N

(d) 850 hPa, 56°-60°N

Figure B.2: Comparison of the speed distributions of high-amplitude and lower-amplitude waves at 850 hPa. The decreasing tendency is most visible in the eastward propagation speed.

Appendix C

Speed trends in early- and late-period heatwaves

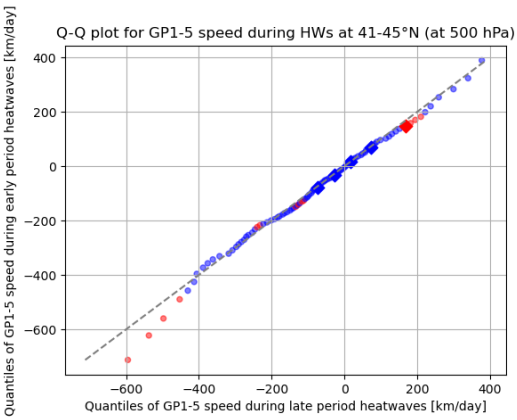

(a) 500 hPa, 41°-45°N

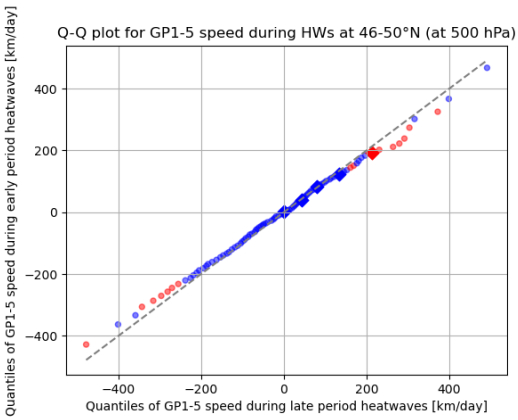

(b) 500 hPa, 46°-50°N

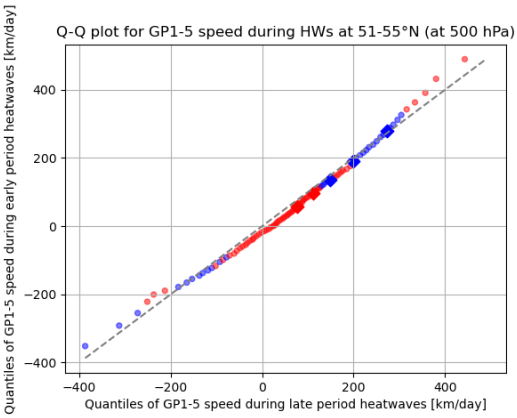

(c) 500 hPa, 51°-55°N

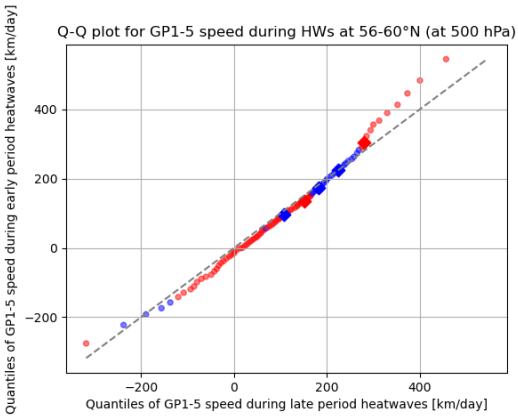

(d) 500 hPa, 56°-60°N

Figure C.1: Comparing the distributions of GP1–5 speed at 500 hPa on the heatwave days of the early period (1979–2010) and the late period (2010-2022).

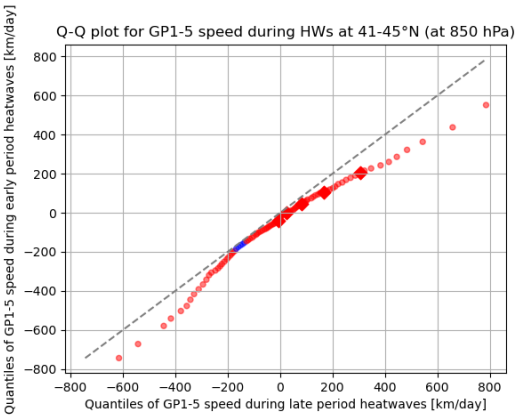

(a) 500 hPa, 41°-45°N

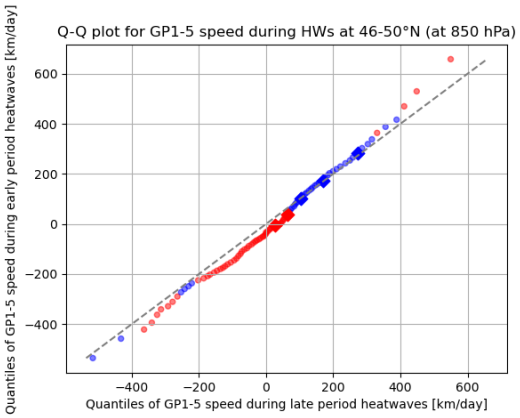

(b) 500 hPa, 46°-50°N

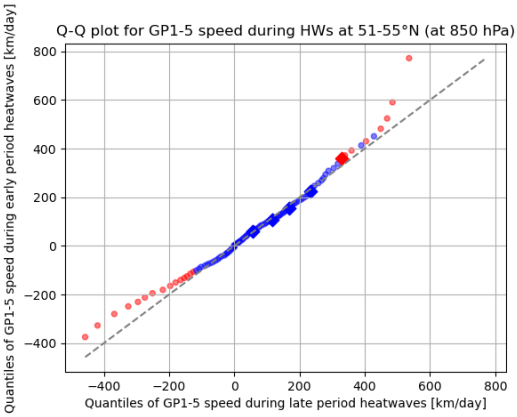

(c) 500 hPa, 51°-55°N

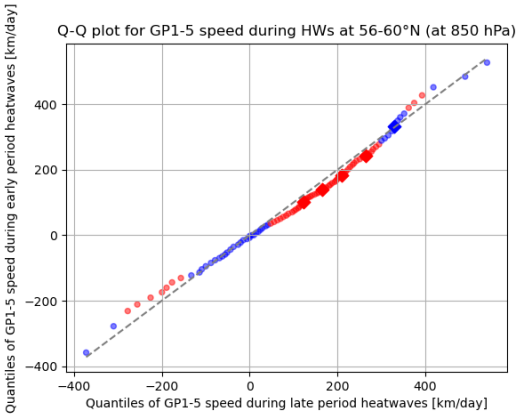

(d) 500 hPa, 56°-60°N

Figure C.2: Comparing the distributions of GP1–5 speed at 850 hPa on the heatwave days of the early period (1979–2010) and the late period (2010-2022).

Bibliography

[1] Elizabeth Barnes and James Screen. "The impact of Arctic warming on the mid-latitude jet-stream: Can it? Has it? Will it?" In: *Wiley Interdisciplinary Reviews: Climate Change* 6 (Mar. 2015). DOI: 10.1002/wcc.337.

[2] Elizabeth A. Barnes. "Revisiting the evidence linking Arctic amplification to extreme weather in midlatitudes". In: *Geophysical Research Letters* 40.17 (2013), pp. 4734–4739. DOI: https://doi.org/10.1002/grl.50880.

[3] Elizabeth A. Barnes et al. "Exploring recent trends in Northern Hemisphere blocking". In: *Geophysical Research Letters* 41.2 (2014), pp. 638–644. DOI: https://doi.org/10.1002/2013GL058745.

[4] Russell Blackport and James Screen. "Insignificant effect of Arctic amplification on the amplitude of midlatitude atmospheric waves". In: *Science Advances* 6 (Feb. 2020), eaay2880. DOI: 10.1126/sciadv.aay2880.

[5] Judah Cohen, Karl Pfeiffer, and Jennifer Francis. "Warm Arctic episodes linked with increased frequency of extreme winter weather in the United States". In: *Nature Communications* 9 (Mar. 2018). DOI: 10.1038/s41467-018-02992-9.

[6] Judah Cohen et al. "Divergent consensuses on Arctic amplification influence on midlatitude severe winter weather". In: *Nature Climate Change* 10 (Dec. 2019), pp. 1–10. DOI: 10.1038/s41558-019-0662-y.

[7] Judah Cohen et al. "Recent Arctic amplification and extreme mid-latitude weather". In: *Nature Geoscience* 7 (Aug. 2014), pp. 627–637. DOI: 10.1038/ngeo2234.

[8] European Commission and Joint Research Centre. *Drought in Europe: August 2022 – GDO analytical report*. Publications Office of the European Union, 2022. DOI: doi/10.2760/264241.

[9] Dim Coumou, Jascha Lehmann, and Johanna Beckmann. "Climate change. The weakening summer circulation in the Northern Hemisphere mid-latitudes". In: *Science (New York, N.Y.)* 348 (Mar. 2015). DOI: 10.1126/science.1261768.

[10] Dim Coumou and Stefan Rahmstorf. "A Decade of Weather Extremes". In: *Nature Climate Change* 2 (Mar. 2012). DOI: 10.1038/NCLIMATE1452.

[11] Dim Coumou et al. "The influence of Arctic amplification on mid-latitude summer circulation". In: *Nature Communications* 9 (Dec. 2018). DOI: 10.1038/s41467-018-05256-8.

[12] United Nations Office for Disaster Risk Reduction. *The human cost of disasters: an overview of the last 20 years (2000-2019)*. Accessed: 07 May 2023.

[13] Jennifer Francis and S. Vavrus. "Evidence for a wavier jet stream in response to rapid Arctic warming". In: *Environmental Research Letters* 10 (Jan. 2015). DOI: 10.1088/1748-9326/10/1/014005.

[14] Jennifer A. Francis and Stephen J. Vavrus. "Evidence linking Arctic amplification to extreme weather in mid-latitudes". In: *Geophysical Research Letters* 39.6 (2012). DOI: https://doi.org/10.1029/2012GL051000.

[15] R. Graversen and Mattias Burtu. "Arctic amplification enhanced by latent energy transport of atmospheric planetary waves". In: *Quarterly Journal of the Royal Meteorological Society* 142 (Mar. 2016), n/a–n/a. DOI: 10.1002/qj.2802.

[16] Hans Hersbach et al. "The ERA5 global reanalysis". In: *Quarterly Journal of the Royal Meteorological Society* 146.730 (2020), pp. 1999–2049. DOI: https://doi.org/10.1002/qj.3803.

[17] J.R. Holton and G.J. Hakim. *An Introduction to Dynamic Meteorology*. International Geophysics. Elsevier Science, 2013. ISBN: 9780123848666.

[18] IPCC. *Climate Change 2022: Impacts, Adaptation and Vulnerability*. Summary for Policymakers. Cambridge, UK and New York, USA: Cambridge University Press, 2022, pp. 3–33. ISBN: 9781009325844.

[19] Kai Kornhuber and Talia Tamarin-Brodsky. "Future Changes in Northern Hemisphere Summer Weather Persistence Linked to Projected Arctic Warming". In: *Geophysical Research Letters* 48.4 (2021), e2020GL091603. DOI: https://doi.org/10.1029/2020GL091603.

[20] Kai Kornhuber et al. "Amplified Rossby waves enhance risk of concurrent heatwaves in major breadbasket regions". In: *Nature Climate Change* 10 (Jan. 2020), pp. 1–6. DOI: 10.1038/s41558-019-0637-z.

[21] NRK. *Tørke fører til full stans i strømproduksjonen [Drought leads to a complete standstill in electricity production]*. Accessed: 07 May 2023.

[22] Jacopo Riboldi et al. "On the Linkage Between Rossby Wave Phase Speed, Atmospheric Blocking, and Arctic Amplification". In: *Geophysical Research Letters* 47 (Oct. 2020). DOI: 10.1029/2020GL087796.

[23] Simone Russo, Jana Sillmann, and Erich Fischer. "Top ten European heatwaves since 1950 and their occurrence in the coming decades". In: *Environmental Research Letters* 10 (Dec. 2015), p. 124003. DOI: 10.1088/1748-9326/10/12/124003.

[24] Simone Russo et al. "Magnitude of extreme heat waves in present climate and their projection in a warming world". In: *Journal of Geophysical Research Atmospheres* 19 (Nov. 2014), pp. 12500–12512. DOI: 10.1002/2014JD022098.

[25] James Screen and Ian Simmonds. "Amplified mid-latitude planetary waves favour particular regional weather extremes". In: *Nature Climate Change* 4 (June 2014), pp. 704–709. DOI: 10.1038/nclimate2271.

[26] G.K. Vallis. *Atmospheric and Oceanic Fluid Dynamics: Fundamentals and Large-scale Circulation*. Cambridge University Press, 2006. ISBN: 9781139459969.

[27] Ronald E Walpole et al. *Probability and statistics for engineers and scientists*. 9th ed. Pearson, 2010. ISBN: 9780321629111.

[28] *Wavier jet stream 'may drive weather shift'*. https://www.bbc.com/news/science-environment-26023166. Accessed: 20 April 2023.

[29] *WHO: Climate change is already killing us, but strong action now can prevent more deaths*. https://www.who.int/europe/news/item/07-11-2022-statement---climate-change-is-already-killing-us--but-strong-action-now-can-prevent-more-deaths. Accessed: 07 May 2023.

[30] *Windy: Wind map & weather forecast*. windy.com. Retrieved: 28 April 2023.
[31] Philipp Zschenderlein et al. "Large-scale Rossby wave and synoptic-scale dynamic analyses of the unusually late 2016 heatwave over Europe". In: *Weather* 73 (July 2018), pp. 275–283. DOI: 10.1002/wea.3278.
[32] Philipp Zschenderlein et al. "Processes determining heat waves across different European climates". In: *Quarterly Journal of the Royal Meteorological Society* 145 (July 2019), pp. 2973–2989. DOI: 10.1002/qj.3599.